cmgh
CELLULAR AND MOLECULAR GASTROENTEROLOGY AND HEPATOLOGY

ORIGINAL RESEARCH

Hepatocyte-specific Epidermal Growth Factor Receptor Deletion Promotes Fibrosis but has no Effect on Steatosis in Fast-food Diet Model of Metabolic Dysfunction-associated Steatotic Liver Disease

Shehnaz Bano,[1] Matthew A. Copeland,[1] John W. Stoops,[1] Anne Orr,[1] Siddhi Jain,[1] Shirish Paranjpe,[1] Raja Gopal Reddy Mooli,[2] Sadeesh K. Ramakrishnan,[2] Joseph Locker,[1] Wendy M. Mars,[1] George K. Michalopoulos,[1] and Bharat Bhushan[1]

[1]*Department of Pathology and Pittsburgh Liver Research Center, School of Medicine, University of Pittsburgh, Pittsburgh, Pennsylvania; and* [2]*Division of Endocrinology and Metabolism, Department of Medicine, University of Pittsburgh, Pittsburgh, Pennsylvania*

SUMMARY

Hepatocyte-specific epidermal growth factor receptor deletion did not impact steatosis but promoted fibrosis in the murine fast-food diet model of metabolic dysfunction-associated steatotic liver disease. Gene networks associated with lipid metabolism were greatly altered upon epidermal growth factor receptor deletion, but phenotypic effects might be compensated by alternative signaling pathways.

BACKGROUND & AIMS: Metabolic dysfunction-associated steatotic liver disease (MASLD) has become the most prevalent chronic liver disorder, with no approved treatment. Our previous work demonstrated the efficacy of a pan-ErbB inhibitor, Canertinib, in reducing steatosis and fibrosis in a murine fast-food diet (FFD) model of MASLD. The current study explores the effects of hepatocyte-specific ErbB1 (ie, epidermal growth factor receptor [EGFR]) deletion in the FFD model.

METHODS: $EGFR^{flox/flox}$ mice, treated with AAV8-TBG-CRE to delete EGFR specifically in hepatocytes (EGFR-KO), were fed either a chow-diet or FFD for 2 or 5 months.

RESULTS: Hepatocyte-specific EGFR deletion reduced serum triglyceride levels but did not prevent steatosis. Surprisingly, hepatic fibrosis was increased in EGFR-KO mice in the long-term study, which correlated with activation of transforming growth factor-β/fibrosis signaling pathways. Further, nuclear levels of some of the major MASLD regulating transcription factors (SREBP1, PPARγ, PPARα, and HNF4α) were altered in FFD-fed EGFR-KO mice. Transcriptomic analysis revealed significant alteration of lipid metabolism pathways in EGFR-KO mice with changes in several relevant genes, including down-regulation of fatty-acid synthase and induction of lipolysis gene, *Pnpla2*, without impacting overall steatosis. Interestingly, EGFR downstream signaling mediators, including AKT, remain activated in EGFR-KO mice, which correlated with increased activity pattern of other receptor tyrosine kinases, including ErbB3/MET, in transcriptomic analysis. Lastly, Canertinib treatment in EGFR-KO mice, which inhibits all ErbB receptors, successfully reduced steatosis, suggesting the compensatory roles of other ErbB receptors in supporting MASLD without EGFR.

CONCLUSIONS: Hepatocyte-specific EGFR-KO did not impact steatosis, but enhanced fibrosis in the FFD model of MASLD. Gene networks associated with lipid metabolism were greatly altered in EGFR-KO, but phenotypic effects might be compensated by alternate signaling pathways. *(Cell Mol Gastroenterol Hepatol 2024;18:101380; https://doi.org/10.1016/j.jcmgh.2024.101380)*

Keywords: Epidermal Growth Factor Receptor (EGFR); Metabolic Dysfunction-associated Steatotic Liver Disease (MASLD); Receptor Tyrosine-protein Kinase ErbB-3; Transforming Growth Factor-β (TGF-β).

Metabolic dysfunction-associated steatotic liver disease (MASLD) is a major global health issue, characterized by abnormal fat accumulation in the liver, independent of significant alcohol consumption. Affecting approximately 30% of the global population, MASLD poses a substantial health burden and can progress to metabolic

Abbreviations used in this paper: **AAV, adeno-associated virus; ACC, acetyl CoA carboxylase; ACLY, ATP citrate lyase; ALT, alanine aminotransferase; α-SMA, alpha smooth muscle actin; ANOVA, analysis of variance; AST, aspartate aminotransferase; CCl4, carbon tetrachloride; DAVID, Database for Annotation, Visualization and Integrated Discovery; DEG, differentially expressed genes; EGFR, epidermal growth factor receptor; EGFR-KO, Hepatocyte-specific deletion of EGFR; FASN, fatty acid synthase; FFD, fast-food diet; GO, gene ontology; H&E, hematoxylin and eosin; HFD, high-fat diet; HNF4α, hepatocyte nuclear factor 4α; ip, intraperitoneally; IPA, Ingenuity Pathway Analysis; KEGG, Kyoto Encyclopedia of Genes and Genomes; MASH, metabolic dysfunction-associated steatohepatitis; MASLD, metabolic dysfunction-associated steatotic liver disease; MMP, matrix metalloproteinase; PBS, phosphate buffered saline; SCD-1, stearoyl-CoA desaturase; SEM, standard error of the mean; TBG, thyroxine binding globulin; TG, triglyceride; TGF-β, transforming growth factor-β; TIMP, tissue inhibitors of metalloproteinase; TUNEL, terminal deoxynucleotidyl transferase dUTP nick end labeling; WT, wild-type.**

Most current article

2352-345X
https://doi.org/10.1016/j.jcmgh.2024.101380

dysfunction- associated steatohepatitis (MASH), cirrhosis, and hepatocellular carcinoma.[1,2] Despite its prevalence, the detailed molecular pathways driving MASLD progression are only partially understood, and currently there is no approved pharmacological treatment specific for MASLD.[2,3]

Epidermal growth factor receptor (EGFR) or ErbB1 is a transmembrane receptor tyrosine kinase expressed in most organs, including liver, and is integral to numerous cellular processes, including cell proliferation.[4] Other ErbB family members include ErbB2, ErbB3, and ErbB4. Among all ErbB receptors, although only EGFR (ie, ErbB1) and ErbB3 are well known to be expressed in normal adult liver/hepatocytes, ErbB2 is also reported to be expressed in hepatocytes in various liver diseases, including MASH and hepatocellular carcinoma.[5]

EGFR is mostly known for its proliferative/regenerative role in the liver, but its role in liver lipid metabolism is also emerging.[4] An earlier study has reported altered plasma and liver lipid levels, along with increased hepatic expression of fatty acid synthase and its transcriptional regulator SREBP1, in mice with gain-of-function mutation in EGFR kinase domain.[6] Our previous study, serendipitously, identified a role of EGFR in lipid metabolism in regenerating liver, with the observation that inhibition of EGFR drastically reduced transient hepatocyte steatosis following partial hepatectomy.[7] Concomitantly, another study showed similar effects in hepatocyte-specific EGFR-mutant mice (lacking EGFR kinase activity) in the partial hepatectomy model, raising critical questions about EGFR's role in hepatic steatosis in chronic liver diseases.[8]

To explore the role of EGFR in hepatic steatosis during MASLD, we conducted an EGFR inhibition study by employing Canertinib, a pan-ErbB receptor inhibitor, in a mouse model replicating diet-induced MASLD by feeding mice a "fast-food diet" (FFD).[9] Remarkably, Canertinib not only prevented the development of steatosis but also reversed already developed steatosis/fibrosis in long-term studies, suggesting a therapeutic potential. These findings were corroborated by other research groups using potent and selective EGFR inhibitors (PD153035 and AG1478), which showed beneficial effects on steatosis and/or fibrosis in high-fat diet (HFD) models.[10,11]

In this study, we employed a hepatocyte-specific EGFR knockout (KO) murine model to understand the specific impact of EGFR on MASLD phenotype induced by an FFD. Despite significant molecular shifts, including alteration in expression of multiple lipid metabolic enzymes and transcription factors, steatosis prevention in the EGFR-KO mice did not occur. We observed, however, that administration of Canertinib (pan-ErbB inhibitor) in FFD-fed EGFR-KO mice substantially reduced hepatocyte steatosis, suggesting a complementary role of the other hepatocyte ErbB receptors in maintaining the metabolism of the steatotic hepatocytes. Surprisingly, enhanced fibrosis along with activation of stellate cells and transforming growth factor-β (TGF-β) signaling pathway was observed in the EGFR-KO mice compared with control mice in the long-term (5-month) study. Overall, our current study offers insights into the role of EGFR in MASLD utilizing, for the first time, hepatocyte-specific gene deletion strategy.

Results

Hepatocyte-specific EGFR Deletion (EGFR-KO) has no Effect on Steatosis in a 2-month FFD Study

This study was focused on investigating the role of hepatocyte-specific EGFR in MASLD. EGFR was deleted specifically in hepatocytes (EGFR-KO) using AAV8-TBG-CRE and control mice (wild-type [WT]) were administered AAV8-TBG-GFP. EGFR-KO or WT mice were fed either a standard chow diet or an FFD, for 2 months (Figure 1*A*), which is known to induce steatosis.[9] The successful deletion of EGFR protein in the livers of EGFR-KO mice was confirmed through Western blot analysis (Figure 1*B*). To our knowledge, this is the first time EGFR was deleted specifically in hepatocytes of adult mice in acute manner, so we first characterized its effect at basal level (on standard chow diet). EGFR-KO mice on chow diet and their liver appear to be normal in gross and histological examination with normal serum chemistry and liver triglycerides (TGs) (Figure 1*C*–*G*). As expected, WT mice on the FFD exhibited increased liver-to-body weight ratios and pronounced liver steatosis. However, there were no significant differences in these parameters between WT and EGFR-KO mice (as analyzed using hematoxylin and eosin [H&E] and Oil Red O staining along liver triglyceride levels measurements) (Figure 1*C*–*E*). Notably, serum triglyceride levels were significantly reduced in EGFR-KO mice on FFD compared with their WT-FFD counterparts (Figure 1*G*). Other serum parameters such as cholesterol, alanine aminotransferase (ALT), and aspartate aminotransferase (AST) were not significantly different in FFD-fed WT and EGFR-KO mice; however, EGFR KO mice trended to show decreased ALT/AST levels (Figure 1*F* and *G*). Overall, these observations indicate that EGFR deletion, specifically in hepatocytes, does not substantially impact steatosis in the 2-month FFD model.

EGFR Deletion Enhanced Expression of Transcription Factors Associated With Lipid Metabolism Without Affecting Major Fatty Acid Synthesis Enzymes in the 2-month FFD Study

In our previous study, the pan-ErbB inhibitor, Canertinib, decreased expression (at both the protein and mRNA levels) of major enzymes involved in fatty acid synthesis, such as fatty acid synthase (FASN), acetyl CoA carboxylase (ACC), stearoyl-CoA desaturase (SCD-1), and ATP citrate lyase (ACLY), which were induced by FFD.[9] Therefore, in this study, we examined the effects on these enzymes in the EGFR-KO mice. At the transcriptional level, there was a significant decrease in the mRNA levels of *Fasn* in FFD-fed EGFR-KO compared with WT mice (Figure 2*A*), similar to the observation with Canertinib in our previous study.[9] FFD-dependent induction of gene expression of *Acc, Scd-1,* and *Acly* remain unaltered by EGFR deletion (Figure 2*A*). Protein expression of these fatty acid synthesis genes and FASN was similarly increased in FFD-fed WT and EGFR-KO mice compared with chow-fed counterparts, without any

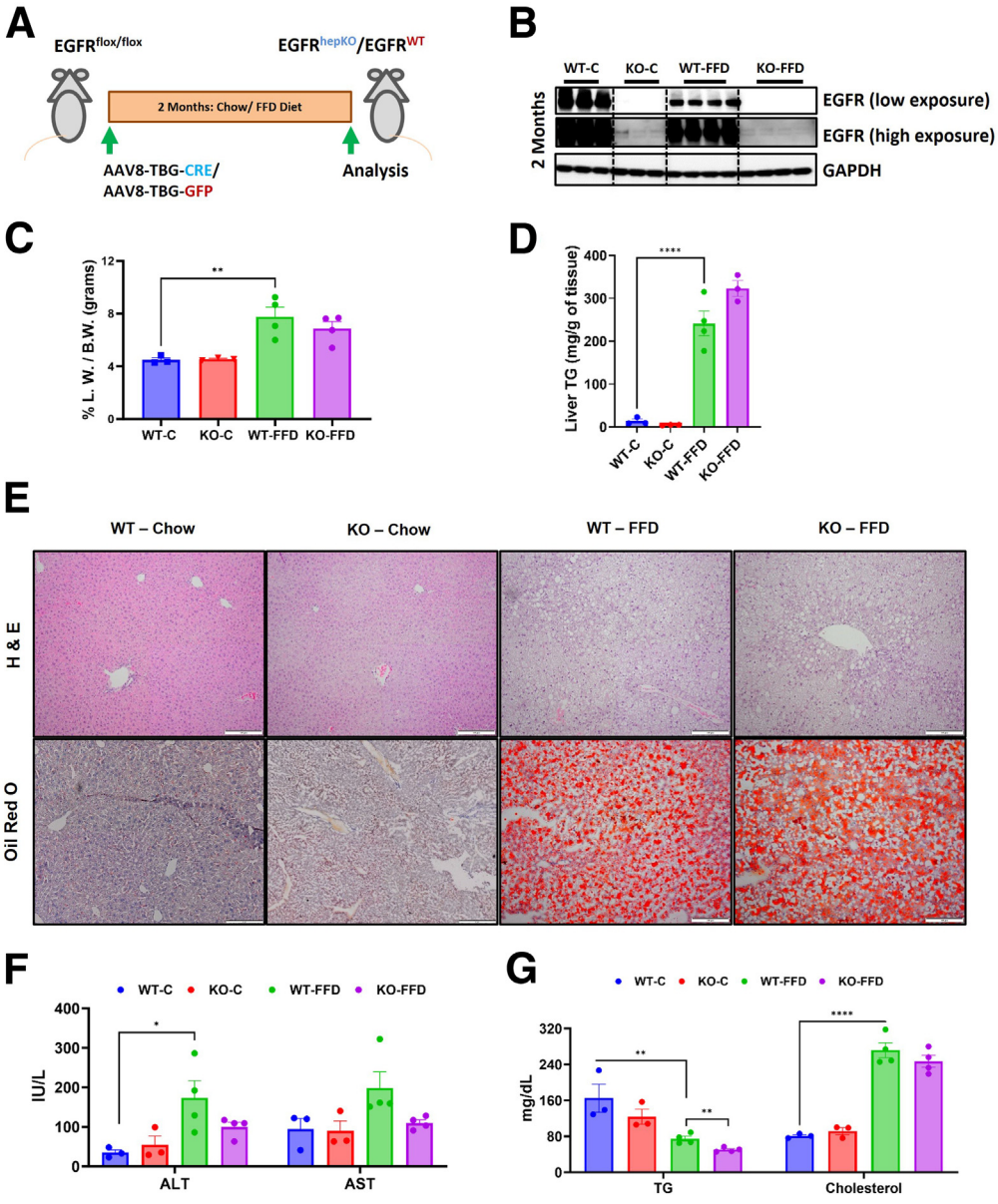

Figure 1. Hepatocyte-specific EGFR deletion did not affect steatosis in a 2-month FFD study. (*A*) Schematics showing 2-month FFD study design. (*B*) Western blot analysis showing successful EGFR deletion using AAV8-TBG-CRE. (*C*) Bar graphs showing liver to body weight ratio at 2 months in chow or FFD-fed WT and EGFR-KO mice. (*D*) Bar graphs showing liver triglycerides levels at 2 months in chow or FFD-fed WT and EGFR-KO mice. (*E*) Representative photomicrographs of H&E (upper panel) and Oil Red O (lower panel) stained liver sections at 2 months in various groups. Bar graphs showing (*F*) ALT, AST, (*G*) cholesterol and TG levels in serum at 2 months in various groups. n = 3–4 mice/group.

significant differences between EGFR-KO and WT mice (Figure 2*B* and *C*). Notably, several of the important lipolysis genes in liver, such as *Pnpla2* and *Ces1g*, showed increased gene expression in FFD-fed EGFR-KO vs WT mice, similar to the effect observed with Canertinib in our previous study (Figure 2*D*).

Further, we investigated the expression status of major transcription factors that regulate fatty acid metabolism in liver (SREBF1, PPARα, and PPARγ) and are known to be induced by FFD. SREBP1 (gene: *Srebf1*) is the major transcriptional regulator of FASN in the liver.[9] *Srebf1* mRNA induction was significantly lower in FFD-fed EGFR-KO mice compared with WT mice (Figure 3*A*). However, SREBP1 nuclear protein levels were significantly higher in FFD-fed EGFR-KO vs WT mice (Figure 3*B* and *C*). Analysis of the RNA sequencing data (described in detail in the next section) using Ingenuity Pathway Analysis (IPA) also indicated increased activation pattern of the SREBP1 downstream gene network in EGFR-KO vs WT mice (Figure 3*D*). PPARγ is another important transcription factor that regulates fatty acid synthesis genes and was found to be affected by ErbB inhibition in our previous study.[9] FFD-driven increase in PPARγ protein expression was also significantly higher in FFD-fed EGFR-KO vs WT mice (Figure 3*B* and *C*). PPARα is a major driver of β-oxidation in liver, and its mRNA and nuclear protein levels were both significantly higher in EGFR-KO vs WT mice in both chow and FFD conditions (Figure 3*A*–*C*). Interestingly, HNF4α protein expression, which is known to negatively regulate steatosis and is downregulated by FFD, was significantly increased in FFD-fed EGFR-KO mice compared with WT mice (Figure 3*B* and *C*), consistent with our findings with Canertinib in our

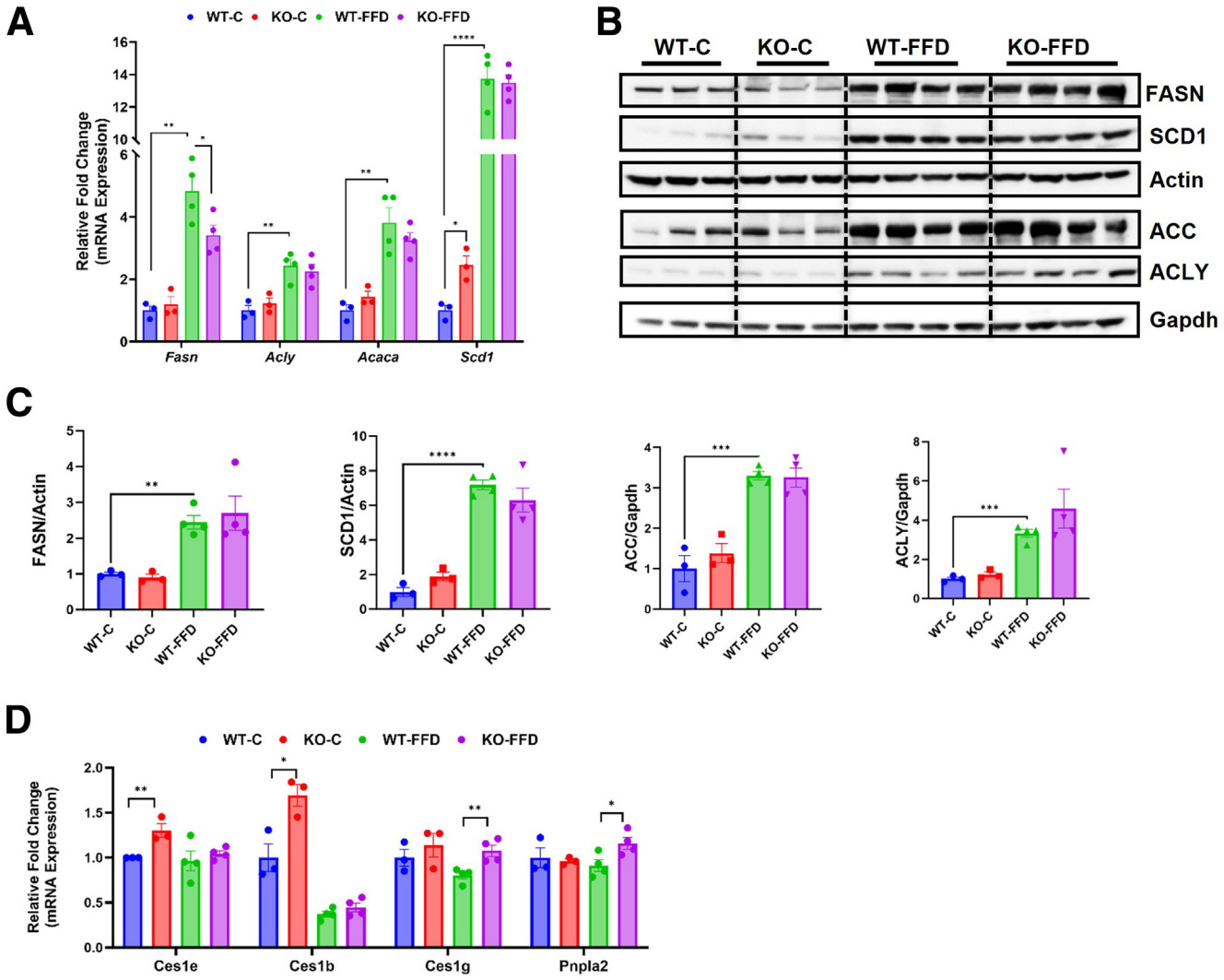

Figure 2. EGFR deletion has no effect on major fatty acid synthesis enzymes in the 2-month FFD study. (*A*) Relative fold-change in mRNA levels and (*B*) Western blot and (*C*) densitometric analysis showing protein expression of fatty acid synthesis genes—*Fasn*, *Acly*, *Scd-1*, *Acaca* or ACC. (*D*) Relative fold-change in mRNA levels of lipolysis genes – *Ces1b, Ces1e, Ces1g* and *Pnpla2*. n = 3–4 mice/group.

previous study.[9,12] Overall, several major transcription factors which regulate lipid metabolism in liver, both positive (SREBP1 and PPARγ) and negative (PPARα and HNF4α) regulators of liver steatosis, showed enhanced expression in FFD-fed EGFR-KO mice compared with FFD-fed WT mice.

Transcriptomic Analysis Showed Altered Lipid Metabolism and Fibrosis Signaling Pathways in EGFR-KO Mice in the 2-month Study

RNA sequencing was performed to investigate the effects of hepatocyte-specific EGFR deletion at global levels in both chow- and FFD-fed conditions, in an unbiased manner. A total of 1414 genes (247 downregulated and 1167 upregulated) were differentially expressed in chow-fed EGFR-KO vs WT mice at 2 months (top 50 upregulated and downregulated genes are listed in Table 1). IPA of differentially expressed genes (DEGs) revealed hepatic fibrosis/hepatic stellate cell activation as one of the top canonical signaling pathways altered in chow-fed EGFR-KO vs WT mice (Figure 4*A*). Similarly, Database for Annotation, Visualization and Integrated Discovery (DAVID) analysis for altered biological processes (gene ontology [GO] terms) also showed extracellular matrix organization process significantly enriched in EGFR-KO vs WT, along with lipid metabolic process, inflammatory response, and fatty acid metabolic process (Figure 4*B* and *D* and Table 2). Several collagens, TGF-β ligands, matrix metalloproteinases (MMPs), and tissue inhibitors of metalloproteinases (TIMPs) were significantly induced in chow-fed EGFR-KO vs WT mice (Figure 4*D*). To corroborate, TGF-β (one of the major regulators of hepatic fibrosis) was among the topmost upstream regulators predicted to be activated in chow-fed EGFR-KO vs WT (with activation z-score: 4.5 and *P*-value of overlap: 1.5×10^{-26}) (Figure 4*F*). Further, TNF was the topmost upstream regulator predicted to be activated in

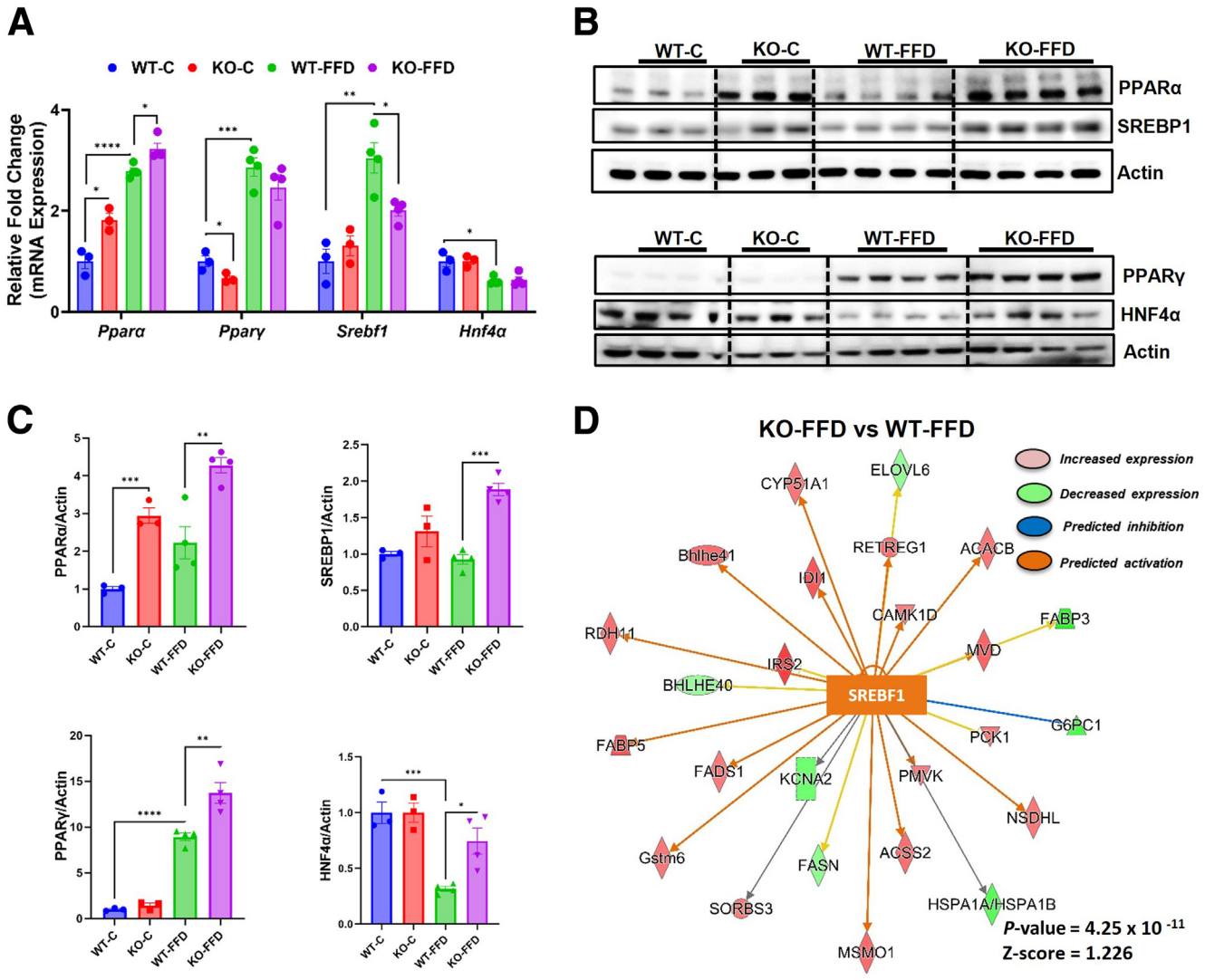

Figure 3. EGFR deletion enhanced expression of lipid metabolism transcription factors in the 2-month FFD study. (*A*) Relative fold-change in mRNA levels, (*B*) Western blot, and (*C*) densitometric analysis showing nuclear protein expression of major transcription factors regulating fatty acid metabolism—SREBP1 (or *Srebf1*), PPARγ, HNF4α, and PPARα. (*D*) IPA analysis of RNA sequencing data showing overall activation pattern of *Srebf1* downstream gene network in EGFR KO-FFD vs WT-FFD group. n = 3–4 mice/group.

chow-fed EGFR-KO vs WT (with activation z-score: 5.2 and *P*-value of overlap: 6.9×10^{-31}), consistent with changes in inflammatory response genes in EGFR-KO mice (Figure 4*F*). It is striking to note that all these changes in gene expression relevant to lipid metabolism, inflammation, and hepatic fibrosis occur in EGFR-KO vs WT mice even at basal level on chow diet without MASLD-inducing FFD.

Similar analysis was also performed in FFD-fed groups. A total of 561 genes (262 downregulated and 299 upregulated) were differentially expressed in FFD-fed EGFR-KO vs WT mice at 2 months (top 50 upregulated and downregulated genes are listed in Table 3). Both IPA (Figure 4*A*) and DAVID analysis (Figure 4*C*) revealed activation of cholesterol biosynthesis processes in EGFR-KO vs WT mice. Further, similar to chow conditions, lipid metabolic process, inflammatory response, and fatty acid metabolic process remain altered in EGFR-KO vs WT mice in 2-month FFD-fed mice, including significant downregulation of important fatty acid synthesis genes such as *Fasn* and *Srebf1* (Figure 4*C* and *E* and Table 2). Similar biological processes/pathways relevant to lipid and glucose metabolism were also found to be altered in Reactome and Kyoto Encyclopedia of Genes and Genomes (KEGG) pathway analysis (Table 4). Overall, our data indicated that hepatocyte-specific EGFR deletion does broadly alter expression of genes involved in steatosis and fibrosis, the hallmark features of MASLD, but does not have an obvious effect on MASLD phenotype in the 2-month study. Although changes in fibrosis gene signature can be observed after 2 months of FFD feeding, it is not sufficient to develop fibrosis phenotype, a key feature that determines outcome in MASLD.[9] No apparent phenotypic evidence of fibrosis was observed at 2

Table 1. Top 50 Genes That Were Up-regulated and Down-regulated in EGFR-KO vs WT Mice on Chow Diet for 2 Months

Up genes	KO/WT 2-month chow	*P* value	Down genes	KO/WT 2−month chow	*P* value
Cyp26b1	11.7	.002	Lars2	−16.3	.007
Osbpl3	6.7	.020	Gm15564	−14.6	.038
Gm32468	5.8	.027	Tmc3	−11.6	.007
Veph1	5.8	.032	Mup15	−9.7	.011
Derl3	5.0	.027	Egfros	−6.9	.009
Cyp2a4	4.9	.037	Ripply1	−6.6	.019
Slc16a5	4.6	.004	Gm49024	−5.9	.010
Gria3	4.6	.007	Sumo2	−5.6	.024
Ntrk2	4.0	.016	Cyp4a31	−5.2	.034
Xlr3a	4.0	.032	Cyp4a10	−5.0	.021
Mfsd2a	3.7	.017	Gm16006	−4.4	.046
Gm42047	3.7	.019	Mup17	−4.2	.018
Sftpa1	3.6	.020	H2-Q2	−4.1	.030
Abcc4	3.4	.000	Mup11	−3.7	.003
Gm28857	3.4	.005	Mup16	−3.7	.005
Efcc1	3.4	.035	Airn	−3.7	.016
Gm47814	3.3	.002	Mogat1	−3.5	.018
Saa1	3.1	.042	Slc34a2	−3.3	.037
Celsr1	3.1	.006	Rcan2	−3.2	.013
Itgax	2.9	.034	Fmr1nb	−3.2	.048
Ntrk1	2.9	.003	Raet1e	−3.2	.024
Kcnk10	2.8	.014	Gm26514	−3.1	.010
Ccr2	2.8	.014	Gm26542	−3.0	.040
Gm31105	2.7	.034	H2-Q1	−3.0	.006
Gm43690	2.7	.007	Acnat2	−2.8	.032
Rab4b	2.7	.002	BC049762	−2.7	.042
Saa3	2.7	.023	Sptb	−2.6	.002
Itk	2.7	.042	1010001B22Rik	−2.6	.035
Zfp462	2.7	.029	Acsm2	−2.6	.020
Cfap100	2.7	.039	Kcnq1ot1	−2.6	.041
Ccdc183	2.6	.009	A330069E16Rik	−2.6	.017
Cct6b	2.6	.007	Gm4876	−2.5	.006
Kcnk5	2.6	.033	Csrp3	−2.5	.018
Gp1ba	2.6	.032	Gm17690	−2.5	.050
Tmem229a	2.6	.044	Gm4952	−2.4	.000
Lrp2	2.6	.026	Chrm3	−2.4	.023
Gm28875	2.6	.024	Avpr1a	−2.4	.025
Tnfrsf25	2.5	.022	Grem2	−2.4	.006
Gm26792	2.5	.035	Gm15956	−2.4	.044
Tlr1	2.5	.036	Dynlt1a	−2.4	.035
Prdm1	2.5	.016	Nr1d1	−2.4	.002
Scd1	2.5	.012	Phf2os1	−2.4	.002
Eif5a2	2.5	.007	Spon2	−2.4	.016
Usp2	2.4	.012	Il4	−2.4	.050
Relt	2.4	.038	Naip1	−2.3	.010
Gprc5b	2.4	.004	Gm10804	−2.2	.023
Omd	2.4	.017	Gm38948	−2.2	.046
Cd79a	2.4	.007	B430010I23Rik	−2.1	.009
Birc5	2.4	.027	Gm16279	−2.1	.044
Lingo4	2.4	.039	Prrx1	−2.1	.046

EGFR-KO, Hepatocyte-specific deletion of EGFR; WT, wild-type.

A

Altered Canonical signaling pathways

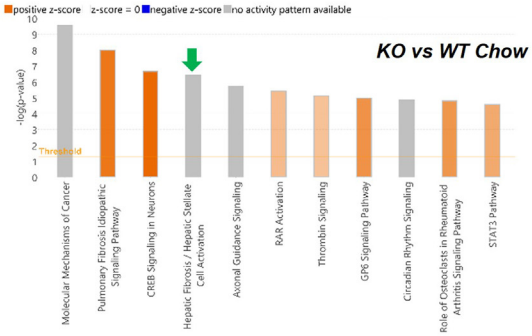

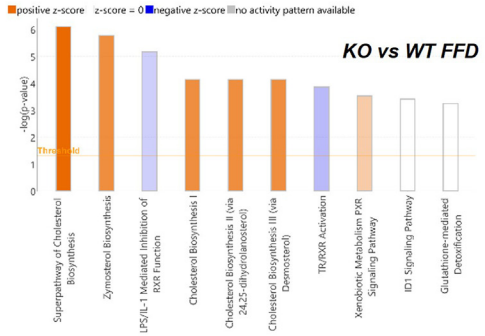

B

Altered Biological processes (GO term)
KO vs WT Chow

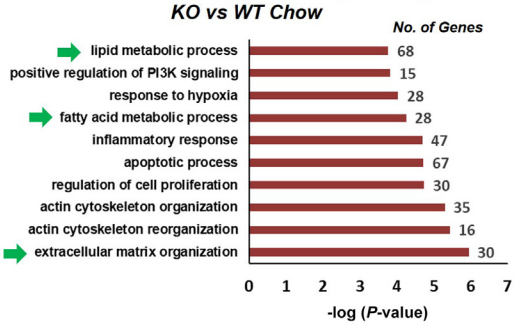

C

Altered Biological processes (GO term)
KO vs WT FFD

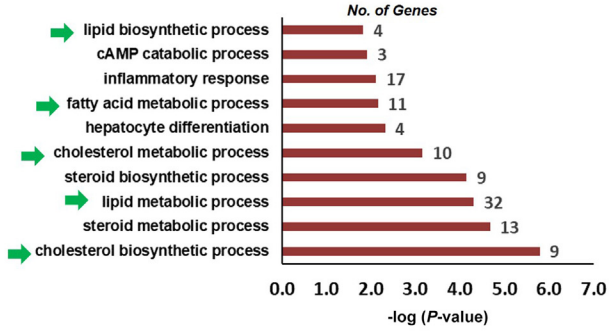

D

Extracellular Matrix Organization Genes altered in KO vs WT (Chow)

Gene Symbol	Relative Fold Change	*P* value
Col14a1	1.6	0.003
Col5a1	1.4	0.04
Col5a2	2.2	0.02
Col16a1	1.6	0.02
Col12a1	0.7	0.01
Col4a5	2.0	0.04
Col4a4	2.1	0.04
Tgfbi	1.3	0.02
Tgfb2	2.2	0.04
Adam9	1.3	0.02
Timp3	1.8	0.01
Mmp23	1.9	0.01
Mmp17	1.7	0.02
Gfap	1.9	0.02
Emilin1	1.6	0.006
Postn	2.0	0.006
Ltbp4	1.5	0.02

E

Lipid Metabolic Process Genes altered in KO vs WT (FFD)

Gene Symbol	Relative Fold Change	*P* value
Fasn	0.7	0.04
Srebf1	0.7	0.02
Elovl6	0.7	0.04
Ces1g	1.3	0.01
Fads1	1.4	0.001
Mvd	1.6	0.004
Fads2	1.3	0.004
Nsdhl	1.4	0.02
Acss2	1.5	0.02
Acacb	1.4	0.01
Mid1ip1	0.6	0.03
Gpd1	0.7	0.008
Fabp5	1.8	0.03
Gpcpd1	1.6	0.01
Cyp1a1	2.6	0.01
Cyp1b1	1.7	0.04
Fabp3	0.1	0.02

F

Altered Upstream Regulators (Top 10)

KO vs WT - CHOW

Upstream Regulator	Activation State	z-score	*P*-value
TNF	Activated	5.2	6.92E-31
AGT	Activated	5.1	7.88E-30
TGFB1	**Activated**	**4.5**	**1.5E-26**
IFNG	Activated	4.4	1.72E-22
IL1B	Activated	3.1	4.25E-16
TP53	Activated	2.8	1.71E-15
STAT3	Activated	4.8	3.18E-15
IL4	Activated	4.6	6.17E-15
IL6	Activated	3.6	1.06E-14
CTNNB1	Activated	2.3	8.66E-14

KO vs WT - FFD

Upstream Regulator	Activation State	z-score	*P*-value
RORA	Inhibited	-2.1	5.75E-12
MAPK7	Activated	2.1	1.06E-09
MAP2K5	Activated	2.07	3.24E-09
HMG20A	Activated	2.6	3.42E-08
SH3TC2	Activated	2.6	9.54E-07
NR1I3	Activated	2.3	8.46E-06
C4BP	Activated	2.0	8.61E-06
FFAR1	Activated	2.2	0.000023
THEM6	Activated	2.4	3.99E-05
ILF3	Inhibited	-2.4	0.00927

Table 2. List of Individual Genes Altered in Selected Biological Processes in the 2-month Study

S. No.	Altered biological process	Gene symbol
1	Fatty acid metabolic process (KO vs WT: Chow)	Hacl1, Hacd1, Hacd4, Elovl2, Acacb, Acsm2, Acot2, Acot6,Acot7, Acnat2, Crot, Cyp4a10, Cyp4a12a, Cyp4a31, Cyp4a32, Fabp2, Fads1, Fads2, Fads6, Ggt5, Lpl, Per2, Ppara, Pparg, Ppard, Pla2g4a, Prkar2b, Scd1
2	Lipid metabolic process (KO vs WT: chow)	Hacl1, Hmgcs1, Hacd1, Hacd4, Arv1, Acap1, Cds2, Elovl2, Asah2, Nsdhl, St3gal5, B4galt5, Acacb, Acsm2, Acss1, Acot2, Acot6, Acot7, Acnat2, Aldh1a1, Aldh1a3, Aox1, Acer2, Adtrp, Crot, Cyp26b1, Cyp4a10, Cyp8b1, Fdft1, Fads1, Fads2, Fads6, Far1, Fmo5, Galc, Gba2, Gstm1, Gstm2, Hsd3b5, Hsd17b2, Ipmk, Inppl1, Inpp5b, Lrat, Lipg, Lipe, Lpin1, Lpl, Msmo1, Mogat1, Nphp3, Neu3, Pnpla6, Pam, Ppara, Ppard, Pi4k2b, Pck1, Pla2g4a, Pltp, Pafah1b3, Plagl2, Retsat, Sds, Sgms1, Scd1, Soat1, Thrsp
3	Inflammatory response (KO vs WT: chow)	Ccl24, Ccr2, Ccr5, Cxcl13, Cx3cr1, Cd14, Cd163, Epha2, F2rl1, Mecom, Naip1, Naip2, Adam8, Agtr1a, Bmp2, Bmp6, C5ar1, C5ar2, Csrp3, Cyp26b1, Cybb, Dab2ip, Fosl2, Ggt5, Havcr2, Hdac7, Irf5, Mfhas1, Nfkb2, Pparg, Ptafr, Pja2, P2rx7, Rps6ka5, Serpinb1a, Stk39, Stab1, Tlr1, Tlr7, Tlr8, Tnfrsf1b, Tnfaip3, Vcam1, Zc3h12a
4	Fatty acid metabolic process (KO vs WT: FFD)	Elovl6, Acacb, Acot11, Cyp1a1, Cyp1b1, Cyp4a32, Fads1, Fasn, Ggt5, Slc27a1, Snca
5	Inflammatory response (KO vs WT: FFD)	Ccr1, Nlrp1a, Nlrp1b, Traf3ip2, Camk1d, Fasn, Fpr1, Ffar4, Ggt5, Il1r1, Lilrb4a, Olr1, Ppbp, Ptger2, Selp, Tbxa2r

EGFR-KO, Hepatocyte-specific deletion of EGFR; FFD, fast-food diet; WT, wild-type.

months in any of the groups. Thus, as a next step, we performed long-term FFD study (5 months), which is known to cause fibrosis.

Hepatocyte-specific EGFR Deletion Increased Fibrosis Without Affecting Steatosis in a 5-month FFD Study

To study the long-term implications of hepatocyte-specific EGFR removal on the progression of MASLD, WT or EGFR-KO mice were either fed a FFD or regular chow diet (as a control) for 5 months (Figure 5*A*). Similar to the 2-month study, the deletion of EGFR protein in the livers of EGFR-KO mice was confirmed through Western blot analysis in the 5-month study (Figure 5*B*). Interestingly, EGFR expression was also decreased by FFD-feeding *per se* in WT mice, but overall EGFR activation (phospho-EGFR/EGFR) appears to be increased by FFD feeding in WT mice (Figure 5*B* and *C*). Hepatocyte-specific EGFR deletion did not alter liver weight, liver triglycerides, or any of the serum parameters (including ALT, AST, cholesterol, and triglycerides) in any of the feeding conditions in the 5-month study (Figure 5*D*–*G*). Further, both EGFR-KO and WT showed overall comparable glucose tolerance and insulin sensitivity after 5 months of FFD (Figure 5*H* and *I*), except a slight but significant increase in glucose levels at 60 minutes after glucose administration in EGFR-KO mice in the glucose tolerance test (Figure 5*H*). No apparent difference was observed in EGFR-KO and WT mice upon examination of H&E and Oil Red O staining in any of the feeding conditions at 5 months, with both groups showing similar steatosis consistent with the liver triglycerides measurements (Figure 5*F*; Figure 6*A* and *B*). Very slight sporadically distributed fibrosis was observed in chow-fed EGFR-KO compared with WT mice, which did not show any signs of fibrosis at 5 months. There were no other apparent differences in gross and histological examinations between these groups on chow diet (Figure 6*A*). However, EGFR-KO mice displayed more prominent fibrosis compared with WT mice after 5 months of FFD feeding, as analyzed using Sirius Red staining (Figure 6*B*). Consistent with increased fibrosis, more activation of stellate cells was observed in FFD-fed EGFR-KO vs WT mice, as analyzed using α-SMA staining (Figure 6*C* and *D*). These changes in fibrosis were consistent with the gene expression changes observed in the earlier 2-month study. Further, 5-month FFD-fed EGFR-KO mice showed slight but significantly higher cell death and compensatory proliferation compared with WT mice as analyzed using Ki67 and terminal deoxynucleotidyl transferase dUTP nick end labeling (TUNEL) staining, respectively (Figure 6*C* and *D*).

All the major fatty acid synthesis enzymes (FASN, ACC, SCD1, and ACLY) remain comparably induced (at both mRNA and protein levels) after FFD in EGFR-KO and WT mice at 5 months (Figure 7*A*–*C*). Further, the major transcription factors that regulate fatty acid metabolism in liver

Figure 4. (***See previous page***). **Transcriptomic analysis showing altered lipid metabolism and fibrosis signaling pathways in EGFR-KO mice in the 2-month FFD study.** (*A*) IPA analysis of differentially expressed genes showing canonical signaling pathways predicted to be altered in EGFR-KO vs WT mice on chow-diet (*left*) or FFD (*right*) for 2 months. (*B and C*) Enrichment analysis using DAVID showing biological processes (GO terms) predicted to be altered in EGFR-KO vs WT mice on (*B*) chow-diet or (*C*) FFD for 2 months. (*D*) List of specific genes related to extracellular matrix organization, which were differentially expressed in EGFR-KO vs WT mice on chow diet. (*E*) List of specific genes related to lipid metabolic process, which were differentially expressed in EGFR-KO vs WT mice on FFD. (*F*) Upstream regulators predicted to be altered in EGFR-KO vs WT mice on chow-diet (*left panel*) or FFD (*right panel*), analyzed using IPA. n = 3–4 mice/group.

Table 3. Top 50 Genes That Were Up-regulated and Down-regulated in EGFR-KO vs WT Mice on FFD for 2 Months

Up genes	KO/WT 2-month FFD	*P* value	Down genes	KO/WT 2−month FFD	*P* value
Gpr68	3.7	.010	AC170998.1	−10.2	.013
Zbtb16	3.4	.003	Fabp3	−7.9	.022
A930028N01Rik	3.4	.031	B4galnt4	−6.7	.021
Galnt12	3.2	.020	Gm16045	−6.6	.017
Prx	2.7	.036	Gm15582	−6.0	.000
Cenpu	2.7	.005	Rbm3os	−5.7	.015
Cyp1a1	2.6	.013	Bhlhe22	−4.7	.017
9330182L06Rik	2.6	.020	Gm14443	−4.6	.007
Prr36	2.5	.0094	Map6	−4.4	.014
Cyp4a32	2.5	.0003	Bst1	−3.5	.030
4732463B04Rik	2.5	.000	Fam57b	−3.0	.002
Igf1os	2.4	.041	Gm26762	−3.0	.022
Azin2	2.4	.008	Asb2	−2.7	.015
Slc26a4	2.3	.019	Gm32098	−2.7	.031
Caprin2	2.3	.047	Trim36	−2.7	.010
C730034F03Rik	2.3	.009	Shisa2	−2.7	.001
Hif3a	2.3	.019	Tpte	−2.7	.010
Nrxn3	2.3	.042	Mtus2	−2.7	.009
R3hdml	2.3	.000	Mns1	−2.6	.027
Plppr5	2.3	.029	9130230L23Rik	−2.6	.022
Cox7a1	2.2	.028	Gm28876	−2.6	.041
Gm11992	2.2	.005	Ccdc142os	−2.5	.046
Gm15835	2.2	.014	Pcdhb5	−2.5	.045
Ift81	2.2	.008	Rflna	−2.5	.049
Chrna4	2.2	.022	Cd160	−2.4	.047
Chrne	2.1	.030	Snca	−2.4	.021
9330020H09Rik	2.1	.012	Rab38	−2.4	.038
Zfp433	2.1	.029	Atp2b2	−2.4	.005
Gm32468	2.1	.032	Cd300e	−2.3	.009
Myom1	2.1	.045	G6pc	−2.3	.001
Gm46411	2.1	.0021	Xlr3b	−2.3	.041
Clip3	2.1	.000	C730002L08Rik	−2.3	.002
Ano5	2.1	.043	Pvrig	−2.3	.031
Fkbp5	2.0	.007	Gm34921	−2.3	.013
Gm11337	2.0	.0448	Rwdd2a	−2.3	.038
Gm17193	2.0	.0001	Tespa1	−2.2	.013
Chil1	2.0	.044	Hspa1a	−2.1	.021
Gm2415	2.0	.042	Cpxm2	−2.1	.027
Irs2	2.0	.001	Mab21l2	−2.1	.017
Snai1	1.9	.041	Cacna1i	−2.1	.023
Epop	1.9	.012	Ltb4r1	−2.1	.003
Rgs16	1.9	.001	Gm20939	−2.1	.023
Gm49012	1.9	.031	Bloc1s1	−2.1	.002
Large2	1.8	.045	Zfp61	−2.0	.013
D630033O11Rik	1.8	.022	Gm35549	−2.0	.035
mt-Atp8	1.8	.005	Dnmt3b	−2.0	.014
Gm10226	1.8	.029	Kbtbd8	−2.0	.005
4833422C13Rik	1.8	.026	Uckl1os	−2.0	.000
Fabp5	1.8	.026	Ifi205	−2.0	.036
Trib3	1.7	.015	9930111J21Rik1	−2.0	.016

EGFR-KO, Hepatocyte-specific deletion of EGFR; FFD, fast-food diet; WT, wild-type.

Table 4. Altered KEGG/Reactome Pathways in the 2-month Study: KO vs WT

KEGG pathway (chow study)	Gene count	*P*−value	KEGG pathway (FFD study)	Gene count	*P*−value
MAPK signaling pathway	39	8.00E−05	Metabolism of xenobiotics by cytochrome P450	8	6.60E−04
PPAR signaling pathway	17	2.00E−04	Chemical carcinogenesis - DNA adducts	8	1.50E−03
Calcium signaling pathway	32	6.00E−04	Insulin resistance	9	1.70E−03
ECM-receptor interaction	16	6.60E−04	Retinol metabolism	8	3.50E−03
AGE-RAGE signaling in diabetic complications	17	8.90E−04	Metabolic pathways	48	5.40E−03
Glucagon signaling pathway	17	1.20E−03	Steroid biosynthesis	4	7.20E−03
Biosynthesis of unsaturated fatty acids	9	1.30E−03	MAPK signaling pathway	14	8.20E−03
AMPK signaling pathway	19	1.60E−03	PPAR signaling pathway	7	9.20E−03
PI3K-Akt signaling pathway	39	3.20E−03	Glutathione metabolism	6	1.50E−02
Insulin resistance	16	5.60E−03	Insulin signaling pathway	8	2.30E−02
Endocrine resistance	14	7.80E−03	AMPK signaling pathway	7	4.40E−02
TNF signaling pathway	16	8.50E−03			
NF-kappa B signaling pathway	15	8.90E−03			

Reactome pathway (chow study)	Gene count	*P*-value	Reactome pathway (FFD study)	Gene count	*P*-value
Signal transduction	220	1.80E−06	Cholesterol biosynthesis	8	1.90E−06
Nuclear receptor transcription pathway	14	6.30E−05	Metabolism of steroids	11	6.70E−04
Collagen biosynthesis and modifying enzymes	15	1.50E−04	G alpha (q) signaling events	13	2.30E−03
Collagen formation	15	1.30E−03	Metabolism of lipids	26	2.50E−03
Extracellular matrix organization	32	1.70E−03	Biological oxidations	12	7.10E−03
MET activates PTK2 signaling	6	1.60E−02	Glutathione conjugation	5	1.00E−02
Signaling by receptor tyrosine kinases	44	1.70E−02	Fatty acid metabolism	10	1.30E−02
Degradation of the extracellular matrix	15	3.40E−02	Signaling by GPCR	23	2.20E−02
Laminin interactions	4	3.70E−02	GPCR downstream signaling	22	2.20E−02
Cell-extracellular matrix interactions	5	3.80E−02	Eicosanoid ligand-binding receptors	3	3.50E−02
Glucose metabolism	12	4.40E−02	Metabolism	51	5.10E−02
ERK/MAPK targets	5	4.60E−02			
Fatty acid metabolism	20	4.80E−02			

EGFR-KO, Hepatocyte-specific deletion of EGFR; FFD, fast-food diet; KEGG: Kyoto Encyclopedia of Genes and Genomes; WT, wild-type.

(*Srebf1*, *Pparα,* and *Pparγ*) remain similarly induced at mRNA after FFD in both EGFR-KO and WT mice (Figure 7*D*). Their protein expression (nuclear level) was also either similar or slightly higher in EGFR-KO vs WT mice, consistent with the findings in the 2-month study (Figure 7*E–F*). Interestingly, hepatocyte nuclear factor 4α (HNF4α) nuclear protein expression, which is known to negatively regulate steatosis and downregulated by FFD, was significantly increased in FFD-fed EGFR-KO mice compared with WT mice (Figure 7*E–F*). Notably, *Hnf4α* mRNA levels were also significantly increased in chow-fed EGFR-KO vs WT mice (Figure 7*D*). This is very interesting, as not much is known about regulators of *Hnf4α* at transcriptional level. The changes in HNF4α protein expression were consistent with the 2-month EGFR-KO study as well as our previously published study with Canertinib,[9] strongly supporting regulation of HNF4α by EGFR. Another notable difference was significant decrease in *Pparγ* mRNA levels in EGFR-KO vs WT mice, only in the chow-fed conditions (Figure 7*D*). However, nuclear protein levels of PPARγ were higher in FFD-fed EGFR-KO vs WT mice (Figure 7*E* and *F*). Lastly, several of the important hepatic fibrosis signaling genes (*Col1a1, Col1a2, Col3a1, Tgfb3, Tgfbr3*), collagen crosslinking genes (*loxl1, loxl2*), and lipolysis genes (*Pnpla2, ces2a* and *ces2c*) were significantly induced in EGFR-KO vs WT mice in chow-fed or FFD-fed conditions (Figure 7*G* and *H*).

Transcriptomic Analysis Revealed Enhanced Hepatic Fibrosis and TGFβ Signaling in EGFR-KO Mice in the 5-month FFD Study

Bulk RNA sequencing was also performed in the 5-month samples to understand the global changes in gene expression profile. Overall, 1706 (712 down and 994 up)

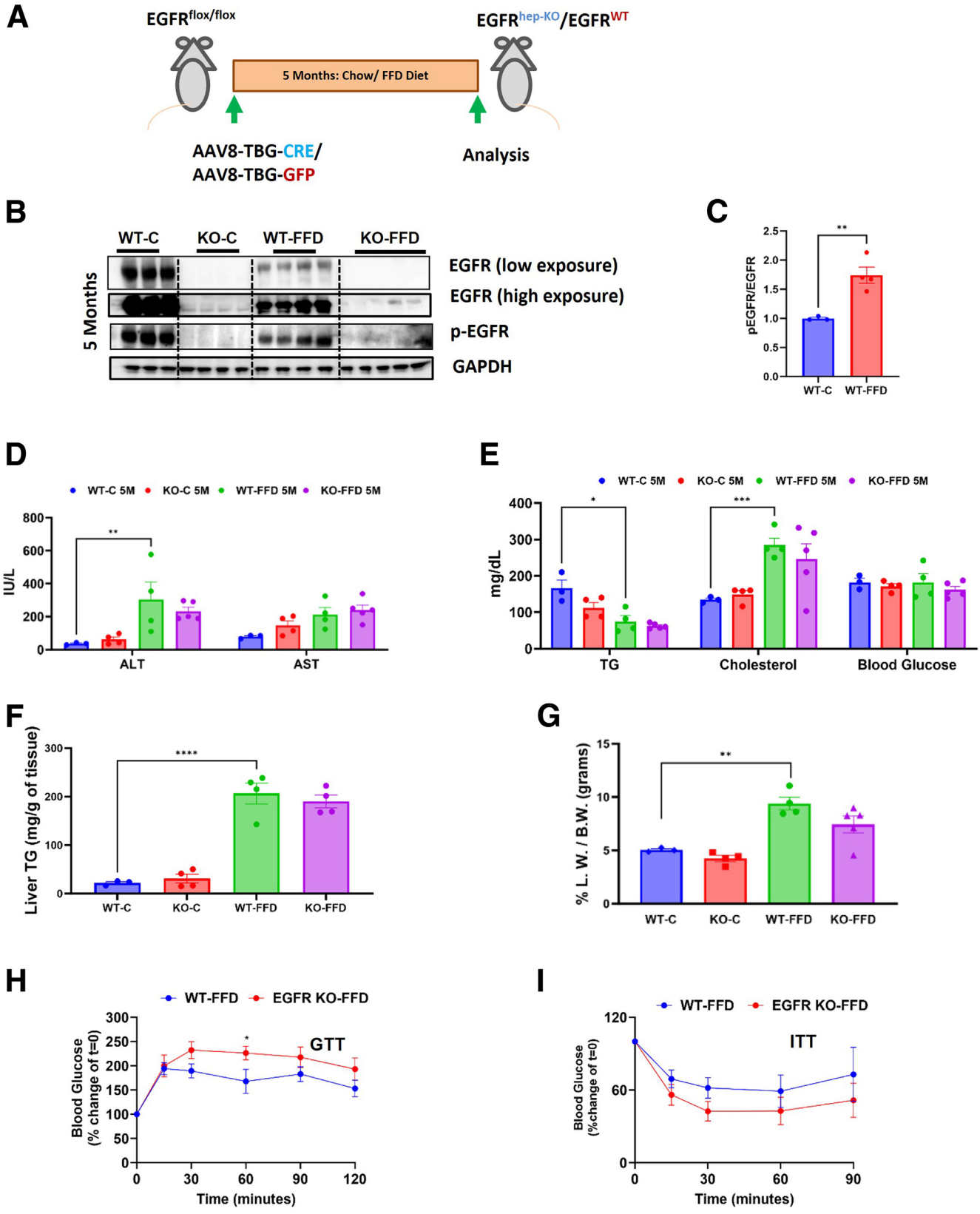

Figure 5. Effects of EGFR deletion in the 5-month FFD study. (*A*) Schematics showing 5-month FFD study design. (*B*) Western blot analysis showing EGFR and p-EGFR expression with densitometric analysis of p-EGFR/EGFR presented in (*C*). Bar graphs showing serum (*D*) ALT and AST, (*E*) cholesterol, TG levels, and blood glucose levels at 5 months in various groups. Bar graphs showing (*F*) liver TG and (*G*) liver to body weight ratio at 5 months in chow or FFD-fed WT and EGFR-KO mice. (*H*) Glucose tolerance test (GTT) data showing blood glucose levels at various time points after glucose administration. (*I*) Insulin tolerance test (ITT) data showing blood glucose levels at various time points after insulin administration. n = 3–5 mice/group.

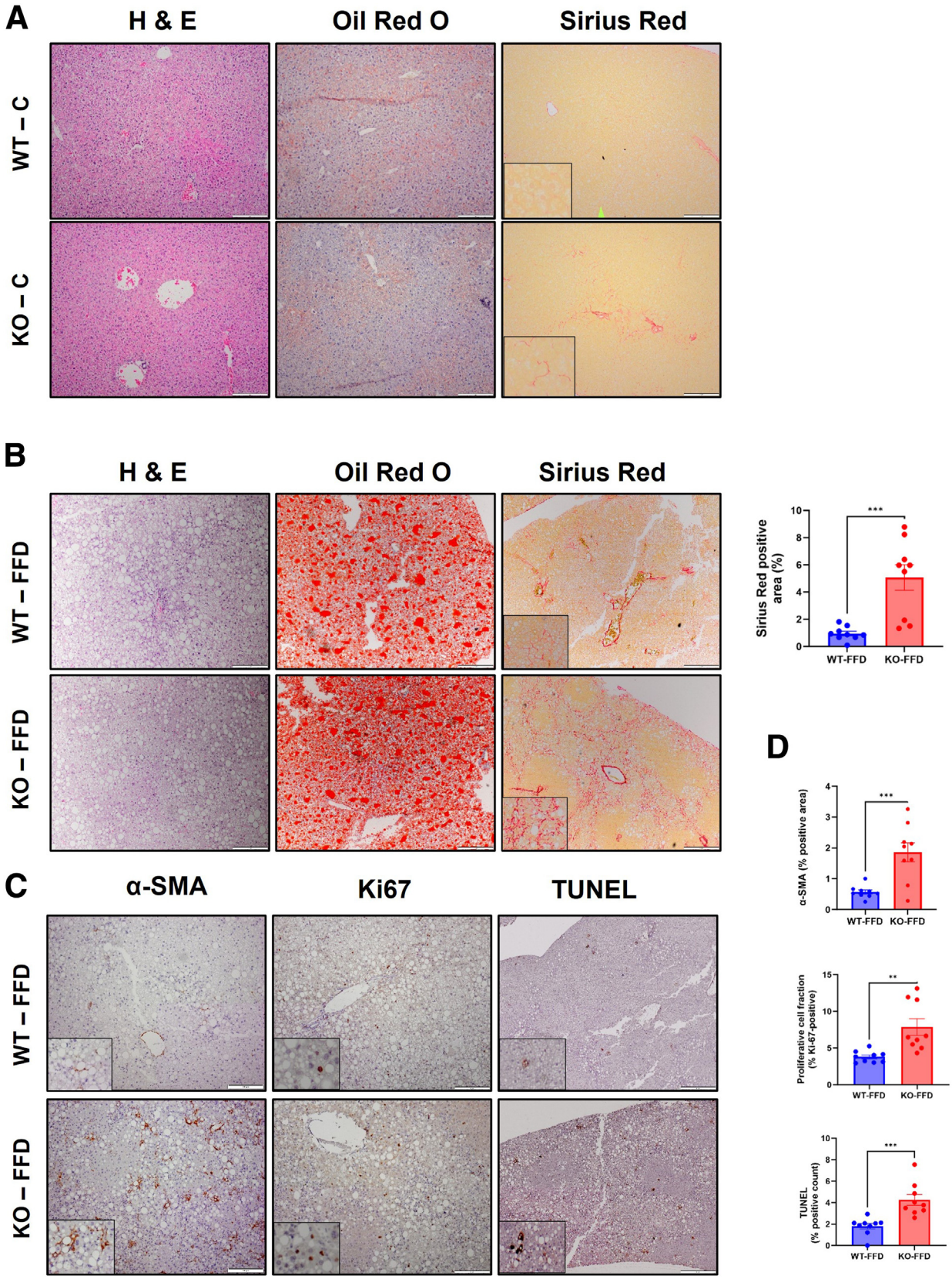
A
H & E
Oil Red O
Sirius Red
WT – C
KO – C
B
H & E
Oil Red O
Sirius Red
WT – FFD
KO – FFD
Sirius Red positive area (%)
WT-FFD
KO-FFD
C
α-SMA
Ki67
TUNEL
WT – FFD
KO – FFD
D
α-SMA (% positive area)
Proliferative cell fraction (% KI-67-positive)
TUNEL (% positive count)

and 707 (274 down and 433 up) genes were differentially expressed in EGFR-KO vs WT mice on chow and FFD, respectively (top 50 upregulated and downregulated genes are listed in Tables 5 and 6). IPA analysis of these DEGs revealed activation of hepatic fibrosis/hepatic stellate cell activation in both chow and FFD conditions in EGFR-KO vs WT mice, consistent with the phenotype of enhanced fibrosis in the KO mice (Figure 8*A* and *C*). This was further highlighted by the fact that TGFβ1 was the topmost upstream regulator predicted to be activated in chow-fed EGFR-KO vs WT mice (with activation z-score of 6.27 and *P*-value of overlap of 5.94×10^{-32}) (Figure 8*B*). Similarly, biological processes/pathways relevant to extracellular matrix organization were also found to be altered in EGFR-KO vs WT mice using GO, Reactome, and KEGG pathway analysis (Table 7). Further, TNF was also among the topmost upstream regulators predicted to be activated (with activation z-score of 5.10 and *P*-value of overlap of 9×10^{-18}) in chow-fed EGFR-KO vs WT mice in IPA analysis (Figure 8*B*), which was consistent with alteration of TNF signaling pathway in KEGG analysis (Table 7), suggesting altered inflammatory response in EGFR-KO mice. Top 10 upstream regulators predicted to be altered in chow or FFD-fed EGFR-KO vs WT mice are provided in Figure 8*B* and *D*. Lastly, comparison analysis of all the canonical signaling pathways (Figure 8*E*) and upstream regulators (Figure 8*F*) between KO and WT was performed at 2 months and 5 months, under both chow and FFD-fed conditions, using IPA. This analysis clearly showed that hepatic fibrosis signaling pathways and its master regulator TGFβ remain consistently activated in EGFR-KO vs WT mice in all the conditions (both 2- and 5-month chow and FFD studies) (Figure 8*E* and *F*). This underpins the robustness of the observed phenotypic and gene expression changes related to fibrosis in EGFR-KO vs WT mice.

Major Signaling Pathways Downstream of ErbB Receptors Remain Intact in EGFR-KO Mice

Overall, our studies indicated EGFR deletion specifically in hepatocytes does not substantially impact steatosis in the FFD model. This is in contrast with our previous findings with the pan-ErbB inhibitor, Canertinib, which prevented steatosis in the FFD model.[9] Strikingly, several relevant and important genes regulating lipid metabolism were altered at transcription level in EGFR-KO mice but did not culminate in changes at the translational and/or phenotypic level. This suggested potential compensation by other similar growth factor signaling pathways in EGFR-KO mice, which regulate common downstream mediators. In our previous study,[9] AKT signaling downstream of EGFR was found to be important for regulating fatty acid metabolism, which was inhibited by Canertinib. Surprisingly, upstream regulator analysis using IPA revealed activation of AKT and PI3K signaling in EGFR-KO vs WT mice, with activation z-score of 4.48 and *P*-value of overlap of 5.75×10^{-7} for PI3K signaling (Figure 9*A* and *B*). Similar was the case of other MAPK mediators downstream of EGFR, such as ERK, p-38, JNK, and RAS (Figure 9*A*). AKT and p-38 phosphorylation were also significantly higher in FFD-fed EGFR-KO mice compared with WT mice, consistent with IPA analysis (Figure 9*D*–*E*). Further, several other growth factor receptors, which can regulate these MAPK signaling similar to EGFR, were predicted to be highly activated in EGFR-KO mice based on downstream gene expression patterns. For instance, gene signatures of NRG1 (ligand of ErbB3 receptor) and HGF remain activated in EGFR-KO vs WT mice (Figure 9*A* and *C*). Protein expression of ErbB3 receptor was also significantly increased in FFD-fed EGFR-KO compared with FFD-fed WT mice, whereas ErbB2 expression also trended to be higher in EGFR-KO mice (Figure 9*F*). Lastly, Met activity (phospho-Met/Met) was increased in chow-fed EGFR-KO vs WT mice. FFD feeding increased Met activity, but it was comparable in FFD-fed EGFR-KO and WT mice (Figure 9*G*). Overall, our data indicated that EGFR downstream signaling was still maintained/activated in EGFR-KO mice (especially AKT signaling), potentially due to compensation by other ErbB family members and/or other receptor tyrosine kinases, which might be the reason for minimal steatosis phenotypic changes in EGFR-KO mice on FFD.

Pan-ErbB Receptor Inhibitor, Canertinib, Prevented Steatosis in EGFR-KO Mice

To investigate whether other ErbB family members might be involved, we administered pan-ErbB inhibitor Canertinib in FFD-fed EGFR-KO mice. As we found previously,[9] the pan-ErbB inhibitor alone was capable of removing hepatocyte steatosis, mere removal of EGFR was not (Figure 10*A* and *B*). Further, we administered Canertinib in FFD-fed EGFR-KO mice for 2 months and noticed that Canertinib removed most of the steatosis even in the complete absence of EGFR (Figure 10*A* and *B*). Even in the absence of EGFR, Canertinib was highly effective in removing the vast majority of steatosis in hepatocytes, with the exception of the immediate pericentral hepatocytes in the lobule (Figure 10*A*). Overall liver triglycerides levels were reduced significantly by Canertinib treatment in both FFD-fed EGFR-KO and WT mice, with no statistically significant difference between WT and EGFR-KO mice (Figure 10*B*).

To further explore this, we conducted a comparative transcriptomic analysis to examine the canonical signaling pathways and upstream regulators altered in EGFR-KO,

Figure 6. (*See previous page*). Hepatocyte-specific EGFR deletion increased fibrosis without affecting steatosis in the 5-month FFD study. (*A*) Representative photomicrographs of H&E, Oil Red O, and Sirius Red stained liver sections at 5 months in chow-fed EGFR-KO and WT mice. (*B*) Representative photomicrographs of H&E, Oil Red O, and Sirius Red-stained liver sections at 5 months in FFD-fed EGFR-KO and WT mice with bar graphs showing quantification of Sirius Red staining on *right panel*. (*C*) Representative photomicrographs of α-SMA, Ki-67, and TUNEL-stained liver sections at 5 months in FFD-fed EGFR-KO and WT mice with quantification in (*D*). n = 3–5 mice/group.

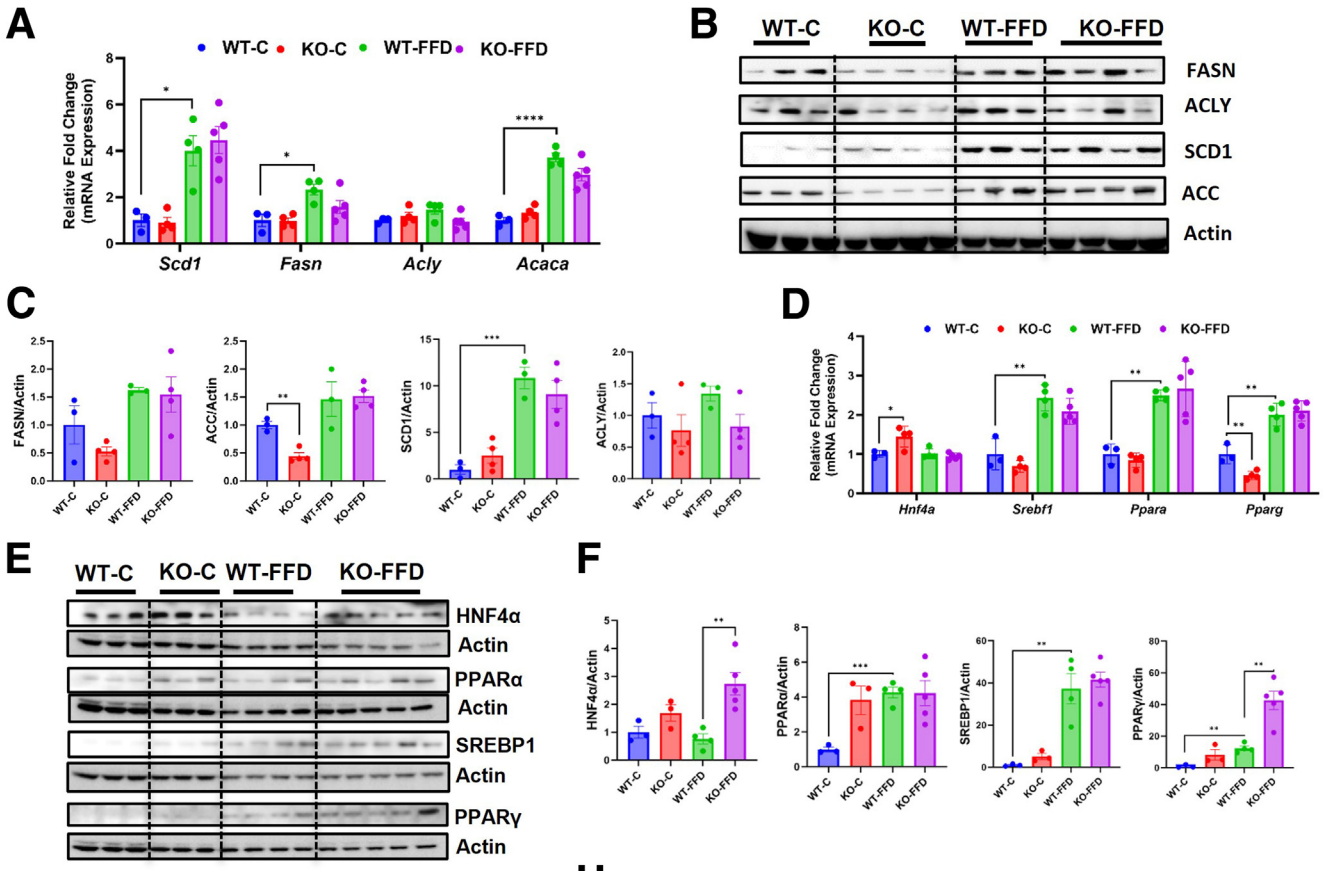

G

Hepatic Fibrosis Signaling/ECM Organization Genes Affected in 5 M Chow (KO vs WT)

Gene Symbol	Relative Fold Change	*P* value
Col27a1	0.6	.030
Col4a1	2.1	.00002
Col4a2	2.0	.00006
Col3a1	2.7	.03
Col6a3	2.5	.0006
Col1a2	3.4	.02
Col1a1	4.9	.01
Col5a1	1.6	.01
Col6a1	2.4	.00002
Col6a2	2.7	.006
Col16a1	1.7	.003
Col11a2	2.7	.03
Tgfbi	1.3	.02
Tgfbr3	1.3	.02
Tgfb3	3.0	.001
Timp3	1.6	.02
Timp2	1.7	.05
Loxl1	2.5	.01
Mmp2	1.7	.01
Loxl2	1.9	.01

H

Hepatic Fibrosis Signaling/ECM Organization Genes Affected in 5 M FFD (KO vs WT)

Gene Symbol	Relative Fold Change	*P* value
Adamtsl4	1.3	.02
Bambi	1.5	.04
Col11a2	0.6	.04
Col13a1	1.4	.004
Tgfbi	1.5	.03
Tgfbr3	1.4	.02
Frem2	4.1	.02
Inhba	0.5	.03
Lamc3	2.6	.03
Lrrc32	1.4	.04
Mansc4	0.6	.010
Mmp11	1.8	.04
Nbl1	2.3	.03
Npnt	0.3	.007
Ltbp4	1.5	.02
Thsd4	2.0	.05

Lipolysis Genes Affected in 5 M FFD (KO vs WT)

Gene Symbol	Relative Fold Change	*P* value
Ces2a	1.5	.02
Pnpla2	1.3	.002
Ces2c	1.6	.02
Pnpla3	0.42	.04

Figure 7. Effects on major fatty acid synthesis enzymes, MASLD-regulating transcription factors, and fibrosis/lipolysis signaling genes in the 5-month FFD study. (*A*) Relative fold-change in mRNA levels, (*B*) Western blot, and (*C*) densitometric analysis of fatty acid synthesis genes—*Fasn*, *Acly*, *Scd-1*, *Acaca* or ACC. (*D*) Relative fold-change in mRNA levels, (*E*) Western blot along with (*F*) densitometric analysis showing nuclear protein expression of major transcription factors regulating fatty acid metabolism—SREBP1 (or *Srebf1*), PPARγ, HNF4α, and PPARα. (*G*) List of specific genes related to hepatic fibrosis signaling and extracellular matrix (ECM) organization, which were differentially expressed in EGFR-KO vs WT mice on chow diet. (*H*) List of specific genes related to hepatic fibrosis/ECM signaling (*left*) and lipolysis (*right*), which were differentially expressed in EGFR-KO vs WT mice on FFD. n = 3–5 mice/group.

Table 5. Top 50 Genes That Were Up-regulated and Down- regulated in EGFR-KO vs WT Mice on Chow Diet for 5 Months

Up genes	KO/WT 5-month chow	*P* value	Down genes	KO/WT 5-month chow	*P* value
Crispld2	12.0	.003	Mas1	−10.0	.001
Thbs1	9.2	.001	Gm5602	−9.3	.001
Ccl2	8.2	.000	Dnah11	−8.6	.004
Derl3	6.3	.000	Gm15441	−7.8	.005
Moxd1	5.6	.007	Phf24	−6.9	.001
Ubd	5.1	.047	Ccdc146	−5.6	.037
Lpl	5.0	.002	Slc22a29	−5.4	.013
Fmn2	5.0	.045	Pkdrej	−5.3	.026
Col1a1	4.9	.007	Gm26813	−5.0	.025
Plat	4.8	.006	Cyp4a14	−4.8	.002
Emp1	4.7	.010	Arg2	−4.6	.009
Plod2	4.7	.008	Mpped2	−4.5	.001
Slc7a1	4.7	.036	Asb16	−4.3	.007
Msln	4.7	.003	Rasl2-9	−4.3	.021
Cpe	4.7	.027	Vldlr	−4.3	.001
Spock2	4.6	.020	Gal3st1	−4.2	.034
Svep1	4.4	.024	Prrx1	−3.8	.010
Rad51c	4.4	.031	Slc26a4	−3.7	.002
Setbp1	4.1	.046	Pnldc1	−3.7	.001
Cbr3	4.0	.005	Gm32872	−3.7	.028
Cd44	4.0	.043	Barhl1	−3.7	.008
Gadd45b	4.0	.010	Acot3	−3.7	.027
Tes	3.9	.011	9530062K07Rik	−3.6	.040
Ptger4	3.9	.046	Esrrg	−3.5	.006
Tmem119	3.8	.013	Gm36908	−3.5	.011
Il1r1	3.8	.027	Rcan2	−3.5	.006
Gm16174	3.8	.001	Obp2a	−3.4	.030
Aebp1	3.7	.000	Sox6os	−3.3	.006
Zbtb16	3.6	.041	Vnn1	−3.3	.026
Fblim1	3.6	.003	Rnf125	−3.2	.019
Ust	3.6	.001	Gm765	−3.1	.045
Sulf1	3.5	.025	Gm21844	−3.0	.034
Nucb2	3.5	.015	Mogat1	−2.9	.003
Fam129c	3.5	.012	Sptb	−2.9	.014
Aoah	3.5	.039	Gdpd3	−2.9	.044
Col1a2	3.4	.015	1810062G17Rik	−2.8	.004
Pirb	3.4	.028	Cyp4a10	−2.8	.000
P2ry6	3.4	.032	Raet1d	−2.7	.001
Lrp2	3.4	.021	Gm34333	−2.7	.023
Igfbp6	3.4	.014	Fam89a	−2.7	.016
Phlda3	3.4	.000	Slc22a3	−2.7	.005
Foxs1	3.4	.009	Cyp26a1	−2.6	.025
Serpinh1	3.3	.000	Srrm4os	−2.6	.002
Gmds	3.2	.018	2310001K24Rik	−2.6	.048
Scara5	3.1	.000	Raet1e	−2.6	.001
Lilrb4a	3.1	.002	Gm33447	−2.6	.017
Serpine1	3.1	.039	Rd3	−2.6	.000
Abcc4	3.0	.000	Rfx4	−2.6	.000
Gpr153	3.0	.006	Adra1a	−2.5	.000
Ezr	3.0	.045	C330021F23Rik	−2.5	.018

EGFR-KO, Hepatocyte-specific deletion of EGFR; WT, wild-type.

Table 6. Top 50 Genes That Were Up-regulated and Down-regulated in EGFR-KO vs WT Mice on FFD for 5 Months

Up genes	KO/WT 5-month FFD	*P* value	Down genes	KO/WT 5-month FFD	*P* value
2010300C02Rik	4.3	.044	Egfr	−4.7	.024
Frem2	4.1	.023	4930544F09Rik	−4.2	.013
Astn1	3.6	.027	AC154762.2	−4.1	.022
Ppp2r2b	3.4	.025	Gm21887	−3.4	.046
Lypd6	3.4	.033	H19	−3.4	.040
Fxyd3	3.3	.048	Cabp2	−3.3	.037
Brd3os	3.3	.014	Gm47283	−3.2	.041
Gprc5a	3.2	.013	Gm26762	−3.2	.037
Bicdl2	3.2	.020	Catsperz	−3.2	.037
Zbtb16	3.0	.013	G6pc	−3.1	.001
Slc12a8	2.9	.020	Fbp2	−3.1	.018
Ubxn10	2.9	.042	Npnt	−3.1	.007
Slc44a4	2.8	.016	Abca14	−3.1	.047
Chn1	2.8	.001	Sall4	−3.1	.037
Lcn8	2.7	.013	Ube4bos1	−3.1	.002
Lrrc15	2.7	.023	4930451E10Rik	−3.0	.014
Osbpl10	2.7	.042	Gm13199	−3.0	.019
Crispld2	2.6	.036	Atp2b2	−2.9	.003
Fam83d	2.6	.019	Gm26779	−2.8	.024
Lamc3	2.6	.037	Gzma	−2.7	.038
Ubash3a	2.5	.049	Gm15401	−2.7	.008
Gm19935	2.5	.042	Tmem267	−2.7	.007
Syt7	2.5	.035	Steap1	−2.7	.025
Efhd1	2.4	.008	Gm45083	−2.6	.005
Tent5b	2.4	.032	Vmn2r20	−2.6	.022
Upp2	2.4	.038	Nap1l5	−2.6	.027
Bdkrb2	2.4	.029	Dmrta1	−2.6	.017
Ncs1	2.4	.020	Ptprn	−2.6	.022
Nbl1	2.3	.031	AA543186	−2.5	.005
Wnt9b	2.2	.034	Dnd1	−2.5	.003
Mok	2.2	.020	Gm48161	−2.5	.033
Slit3	2.2	.014	Gm28836	−2.5	.024
Zfp831	2.2	.042	Gm26584	−2.5	.008
Pgm5	2.2	.017	Gm42679	−2.5	.021
Dusp18	2.2	.032	Tpte	−2.5	.046
Wnt7b	2.2	.044	Pnpla3	−2.4	.046
Oscp1	2.1	.028	Gm44226	−2.4	.027
Ano1	2.1	.013	Igf2bp2	−2.4	.001
Hsd17b6	2.1	.025	Hist1h1d	−2.4	.025
Erbb2	2.0	.029	AC160336.1	−2.4	.038
Lurap1	2.0	.042	Ptges	−2.3	.003
Cyp4a12b	2.0	.013	Dpf3	−2.3	.016
Cyp2a5	2.0	.002	Gpr84	−2.3	.018
A530016L24Rik	2.0	.026	Gm30692	−2.3	.017
Msln	2.0	.022	Hspa1l	−2.3	.018
Dlg2	1.9	.043	Rep15	−2.2	.019
Usp2	1.9	.025	Ppp1r3b	−2.2	.002
Pygm	1.9	.039	Gm21917	−2.2	.031
Mapk8ip1	1.9	.026	Rpl36al	−2.2	.005
Nynrin	1.8	.026	Slc30a10	−2.2	.003

EGFR-KO, Hepatocyte-specific deletion of EGFR; FFD, fast-food diet; WT, wild-type.

A

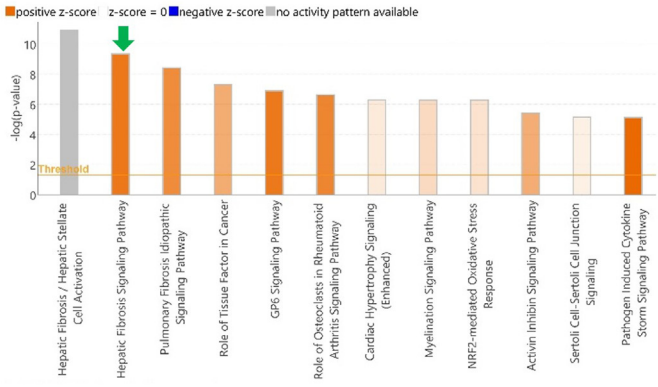

B

Top Upstream Regulators Predicted to be Modulated in KO vs WT: Chow 5 M

Upstream Regulator	Activation State	z-score	p-value
TGFB1	**Activated**	**6.27**	**5.94E-32**
TP53	Activated	3.41	7.94E-26
AGT	Activated	7.18	2.16E-22
CCR2	Activated	4.91	1.28E-20
PPARA	Inhibited	-4.79	8.18E-18
TNF	Activated	5.10	9E-18
IFNG	Activated	4.94	1.38E-17
EGF	Activated	3.94	4.21E-17
F2	Activated	6.31	6.6E-17
IL2	Activated	4.03	6.05E-16

C

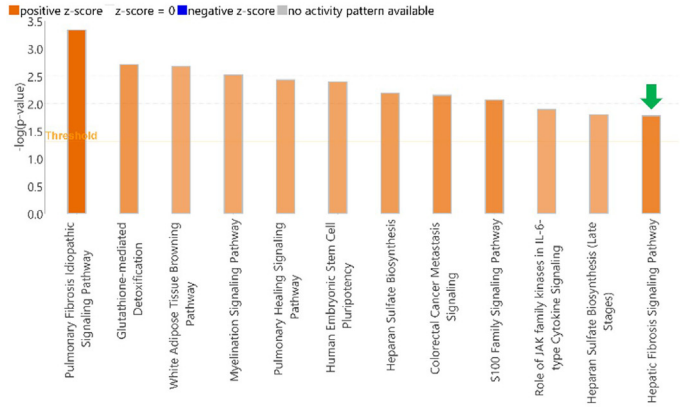

D

Top Upstream Regulators Predicted to be Modulated in KO vs WT: FFD 5 M

Upstream Regulator	Activation State	z-score	p-value
AGT	Activated	2.15	1.24E-12
VEGFA	Activated	2.73	3.49E-07
EZH2	Inhibited	-2.18	4.37E-07
TP73	Activated	2.05	1.21E-05
SORL1	Activated	2.13	3.48E-05
PRL	Activated	2.07	4.01E-05
KLF4	Activated	2.72	4.99E-05
CYP19A1	Activated	2.77	9.93E-05
JUN	Activated	2.41	0.000117
ALDH1A2	Inhibited	-2.43	0.000118

E

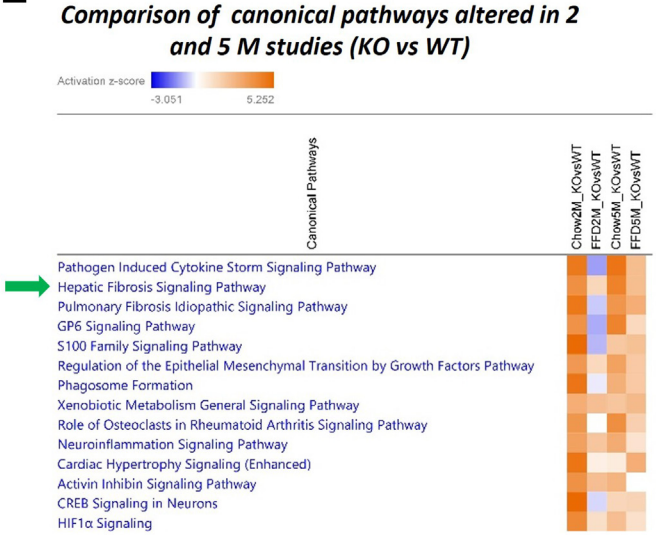

F

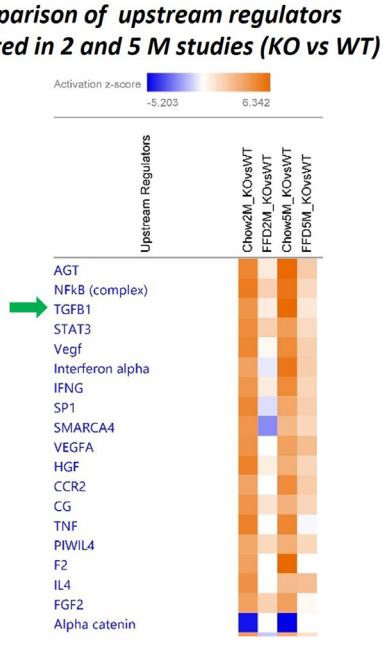

Figure 8. Transcriptomic analysis revealed enhanced hepatic fibrosis and TGF-β signaling in EGFR-KO mice in the 5-month FFD study. IPA analysis of differentially expressed genes showing canonical signaling pathways predicted to be altered in EGFR-KO vs WT mice on (*A*) chow diet and (*C*) FFD for 5 months. IPA analysis showing upstream regulators predicted to be altered in EGFR-KO vs WT mice on (*B*) chow diet and (*D*) FFD for 5 months. (*E and F*) Heatmaps showing comparative analysis of (*E*) canonical signaling pathways and (*F*) upstream regulators predicted to be altered in EGFR-KO vs WT mice on chow diet or FFD for 2 or 5 months.

Table 7. Altered Biological Processes/Pathways: KO vs WT in 5-month Study

GO term (chow study)	Gene count	*P*-value	GO term (FFD study)	Gene count	*P*-value
extracellular matrix organization	35	2.00E−07	cell adhesion	42	1.20E−07
actin cytoskeleton organization	42	4.00E−07	positive regulation of cell migration	23	4.10E−06
positive regulation of cell migration	43	7.30E−07	extracellular matrix organization	18	.000012
collagen fibril organization	17	1.40E−06	negative regulation of cell proliferation	28	.000053
cell adhesion	76	.000002	negative regulation of ERK1 and ERK2 cascade	10	.0006
lipid metabolic process	83	.000015	positive regulation of protein phosphorylation	18	.0013
fatty acid metabolic process	32	.000034	Cell-matrix adhesion	10	.0011
apoptotic process	75	.000058	wound healing	10	.0029
positive regulation of fat cell differentiation	14	.00008	receptor tyrosine kinase signaling pathway	10	.0054
cellular response to low-density lipoprotein particle stimulus	9	.00015	cell proliferation	19	.0082

KEGG pathway (chow study)	Gene count	*P*-value	KEGG pathway (FFD study)	Gene count	*P*-value
PPAR signaling pathway	21	1.70E−05	HIF-1 signaling pathway	11	9.70E−04
PI3K-Akt signaling pathway	53	2.20E−05	MAPK signaling pathway	18	3.10E−03
Metabolic pathways	170	5.80E−05	TGF-beta signaling pathway	9	9.50E−03
Drug metabolism - other enzymes	18	6.40E−04	Hippo signaling pathway	11	9.80E−03
MAPK signaling pathway	40	1.60E−03	Insulin signaling pathway	9	3.40E−02
AGE-RAGE signaling in diabetic complications	18	2.40E−03	Drug metabolism - other enzymes	7	3.40E−02
Lipid and atherosclerosis	30	3.70E−03	PI3K-Akt signaling pathway	17	3.70E−02
Retinol metabolism	17	3.90E−03	Central carbon metabolism in cancer	6	3.80E−02
Protein processing in endoplasmic reticulum	25	4.50E−03	Glutathione metabolism	6	4.40E−02
TGF-beta signaling pathway	17	1.30E−02	Fluid shear stress and atherosclerosis	9	4.50E−02
TNF signaling pathway	17	2.00E−02	Retinol metabolism	7	4.60E−02
Fatty acid degradation	10	2.00E−02			

Reactome pathway (chow study)	Gene count	*P*-value	Reactome pathway (FFD study)	Gene count	*P*-value
Extracellular matrix organization	48	6.00E−08	PKR-mediated signaling	7	1.20E−02
Collagen biosynthesis and modifying enzymes	18	1.40E−05	Molecules associated with elastic fibres	5	1.40E−02
Collagen formation	20	1.70E−05	Signaling by Receptor Tyrosine Kinases	21	1.60E−02
RHO GTPase cycle	52	5.40E−03	Netrin-1 signaling	4	1.80E−02
MET activates PTK2 signaling	7	6.80E−03	Antiviral mechanism by IFN-stimulated genes	8	1.90E−02
Metabolism of carbohydrates	37	7.30E−03	Extracellular matrix organization	14	2.00E−02
NRAGE signals death through JNK	11	9.40E−03	TGF-beta receptor signaling activates SMADs	5	2.20E−02
Signaling by receptor tyrosine kinases	51	1.10E−02	Prostanoid ligand receptors	3	2.20E−02
Signaling by PTK6	10	2.30E−02	Elastic fibre formation	5	2.80E−02
Signaling by non-receptor tyrosine kinases	10	2.30E−02	Signal Transduction	79	2.90E−02
Regulation of IGF transport and uptake by IGFBPs	18	4.10E−02	ERBB2 Activates PTK6 Signaling	3	4.10E−02

EGFR-KO, Hepatocyte-specific deletion of EGFR; FFD, fast-food diet; GO, gene ontology; KEGG, Kyoto Encyclopedia of Genes and Genomes; WT, wild-type.

A

KO vs WT 5M

Upstream Regulator	Activation State	z-score	*P*-value
PI3K (complex)	Activated	4.4	5.75E-07
ERK	Activated	3.9	1.14E-05
P38 MAPK	Activated	3.9	2.41E-05
NRG1	Activated	3.6	0.000016
HGF	Activated	3.3	3.19E-08
RAS	Activated	2.7	0.00211
AKT1	Activated	2.7	7.47E-06
Jnk	Activated	2.4	0.000556
p70 S6k	Activated	2.2	0.00242

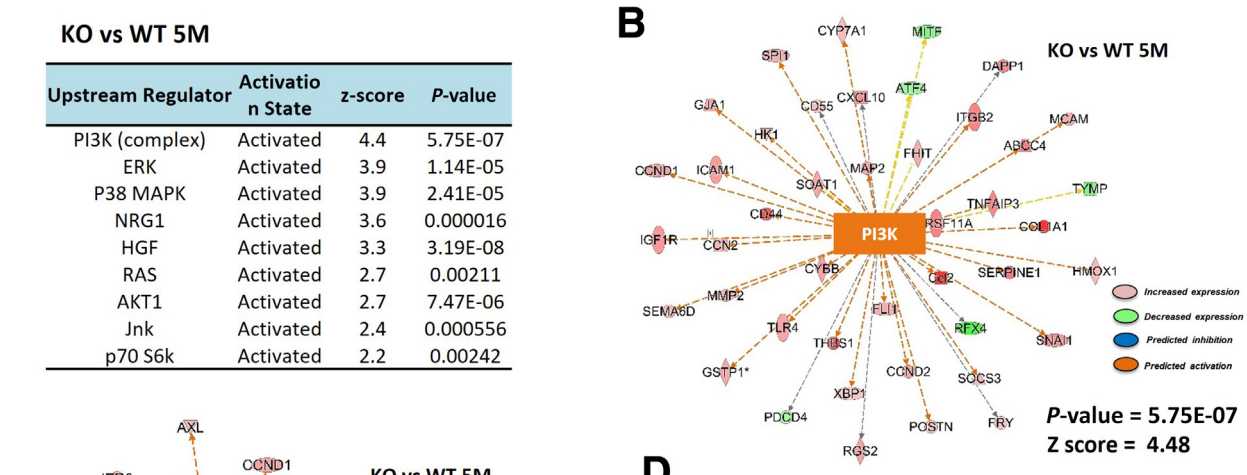

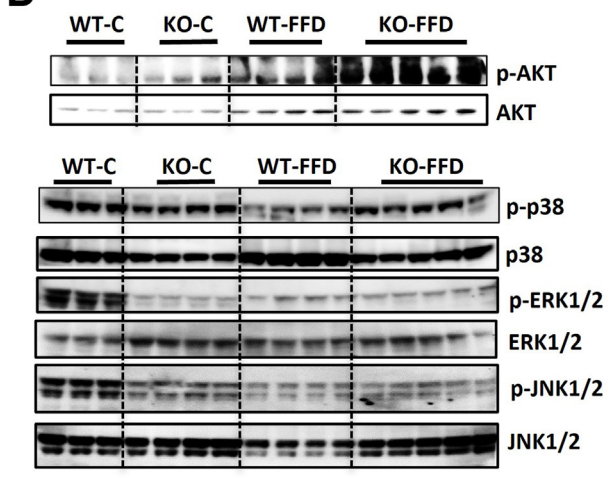

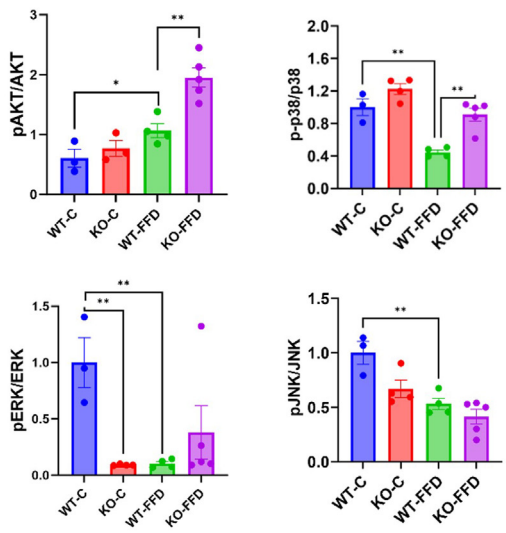

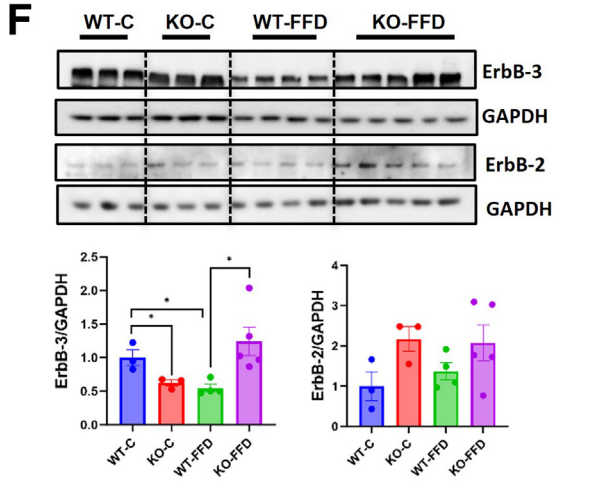

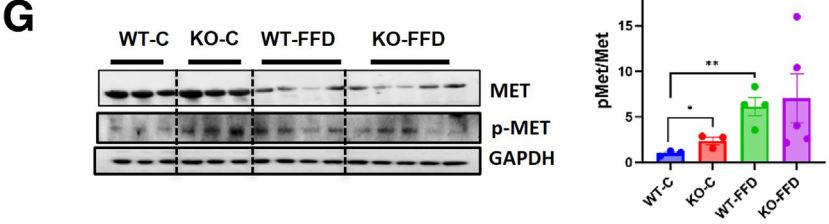

Canertinib-treated WT, and Canertinib-treated EGFR-KO mice all fed FFD, in comparison to FFD-fed WT mice (Figure 10*C* and *D*). Our data highlighted that growth factor signaling (ErbB signaling and ErbB2-ErbB3 signaling) along with downstream MAPK signaling (ERK, RAF, PI3K, AKT) were predicted to be inhibited only in the Canertinib groups, but not the EGFR-KO alone group (Figure 10*C* and *D*). This corresponded with inhibited fatty acid synthesis and fibrosis pathways in the Canertinib groups, but not in the EGFR-KO group (Figure 10*C* and *D*). We further analyzed the overlap of DEGs in Canertinib-FFD-WT/FFD-WT vs Canertinib-FFD-KO/FFD-KO groups to investigate the difference in genes altered by Canertinib in KO vs WT mice (Figure 10*E*). A total of 1794 genes (537 up and 1257 down) were differentially regulated by Canertinib exclusively in FFD-fed WT mice, but not in EGFR-KO mice, indicating these genes were regulated by Canertinib in EGFR-dependent manner (Figure 10*E*). Similarly, 562 genes (230 up and 332 down; top 50 listed in Table 8) were differentially regulated by Canertinib only in EGFR-KO mice, indicating that Canertinib utilizes different sets of genes in EGFR-KO mice to regulate the MASLD phenotype. Indeed, IPA analysis of these 562 genes revealed inhibition of cholesterol biosynthesis, stearate biosynthesis, and collagen biosynthesis as top altered canonical pathways (Figure 10*F*). Further, DAVID analysis of these genes revealed lipid metabolic processes and cholesterol metabolic processes and cellular response to insulin stimulus among significantly enriched biological processes in this gene set (Figure 10*G* and Table 9). Similarly, biological processes/pathways relevant to lipid and cholesterol metabolism were also found to be enriched in this gene-set using Reactome and KEGG pathway analysis (Table 10). This indicates that Canertinib might be utilizing different sets of genes in EGFR-KO conditions to produce phenotype effects on steatosis similar to WT mice.

Discussion

EGFR (ie, ErbB1) is well known for its proliferative role in liver, but its role in lipid metabolism is also emerging. In our previous study, the pan-ErbB inhibitor, Canertinib, drastically reduced steatosis and fibrosis in a murine FFD model of MASLD.[9] Concomitantly, other studies using EGFR inhibitors with different selectivity profiles also demonstrated similar findings in HFD-induced MASLD models, corroborating the relevance of our findings.[10,11] Our current study is very crucial on this topic because it, for the first time, to our knowledge, utilizes hepatocyte-specific gene deletion approach in adult mice to investigate the role of EGFR in MASLD. To our surprise, hepatocyte-specific EGFR deletion had no effect on steatosis but enhanced fibrosis, contrary to our results with Canertinib in our previous study.[9]

Although gross steatosis was not much impacted by hepatocyte-specific EGFR deletion, it was striking to note that, at the molecular level, gene networks and pathways related to lipid metabolism were vastly affected by EGFR deletion. For instance, a key *de novo* fatty acid synthesis gene (ie, FASN) along with its transcription regulator (*Srebf1*) were significantly downregulated, and major hepatic lipase (ie, *Pnpla2*) along with the master regulator of hepatic β-oxidation (ie, *Ppar*α) were significantly upregulated in FFD-fed EGFR-KO mice. Further, nuclear levels of some of the major transcription factors, which inhibit steatosis, such as PPARα and HNF4α, were increased in EGFR-KO mice. All these changes in gene/protein expression were very consistent with our finding with Canertinib in our previous study, which decreased steatosis.[9] However, protein expression of several other fatty acid synthesis enzymes and steatosis-inducing transcription factors (ie, PPARγ and SREBP1) were either unaffected or increased in EGFR-KO mice, which was different from our results with Canertinib in the previous study.[9] Differential activation of some of these interconnected lipid metabolic pathways might be responsible for maintaining the overall "cybernetic" aspects of signaling required to preserve the steatotic phenotype in EGFR-KO mice.

With respect to signaling mediators, inhibition of AKT signaling was found to be important for elimination of steatosis by Canertinib in our previous study.[9] Surprisingly, AKT and other important EGFR downstream signaling mediators remain activated in EGFR-KO mice in the current study. This suggested potential compensation by other functionally similar receptor tyrosine kinases or signaling proteins, such as other ErbB family members or non-ErbB kinases/phosphatases in EGFR-KO mice, which regulate these common downstream mediators. Indeed, increased activity pattern of functionally similar growth factor receptor signaling, including Nrg1/ErbB3 and HGF/MET, was observed in EGFR-KO mice, indicating potential compensation by these receptors. Overall, our data indicated that a major part of EGFR downstream signaling was still maintained in EGFR-KO mice, due to potential compensation by other functionally similar receptors, which might be the reason for minimal steatosis phenotypic changes in absence of EGFR. Indeed, concomitant inhibition of all the ErbB

Figure 9. (***See previous page***). **Major signaling pathways downstream of ErbB receptors remain intact in EGFR KO mice.** (*A*) Upstream regulator analysis using IPA showing major downstream signaling mediators of ErbB signaling (PI3K/AKT, ERK, p70 S6K, Jnk, RAS), and growth factor signaling via NRG1 (ligand for ErbB3) and HGF predicted to be activated in EGFR-KO mice at 5 months. IPA analysis of RNA sequencing data showing predicted activation of (*B*) PI3K and (*C*) NRG1 downstream network in EGFR KO vs WT mice at 5 months. Positive z-scores represents predicted activation of upstream regulator (absolute z-score $>$ 2 considered as significant) based on expression profile of downstream genes. (*D*) Western blot and (*E*) densitometric analysis of total p-38, AKT, ERK, and JNK along with their phosphorylation forms in WT and EGFR KO mice at 5 months. (*F*) Western blot along with densitometric analysis showing protein expression of total ErbB2 and ErbB3 in WT and EGFR-KO mice at 5 months. (*G*) Western blot and densitometric analysis of phospho-MET and MET in EGFR-KO mice at 5 months. n = 3–5 mice/group.

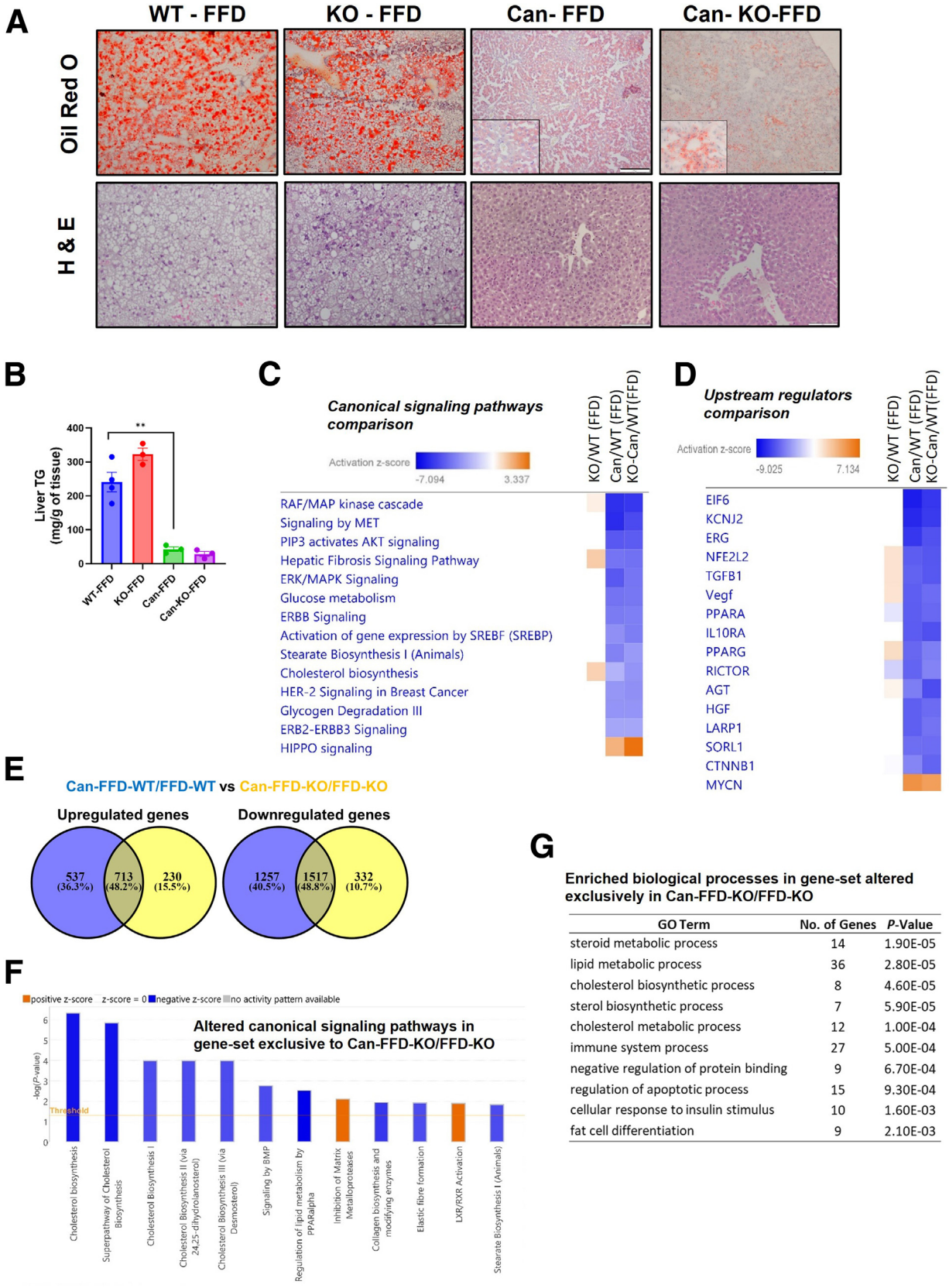

G

Enriched biological processes in gene-set altered exclusively in Can-FFD-KO/FFD-KO

GO Term	No. of Genes	*P*-Value
steroid metabolic process	14	1.90E-05
lipid metabolic process	36	2.80E-05
cholesterol biosynthetic process	8	4.60E-05
sterol biosynthetic process	7	5.90E-05
cholesterol metabolic process	12	1.00E-04
immune system process	27	5.00E-04
negative regulation of protein binding	9	6.70E-04
regulation of apoptotic process	15	9.30E-04
cellular response to insulin stimulus	10	1.60E-03
fat cell differentiation	9	2.10E-03

receptors with Canertinib was effective in drastically reducing steatosis in the EGFR-KO mice. Similar phenomena have been observed in other models as well, where deletion of EGFR and ErbB3 in combination (ie, EGFR/ErbB3 double KO) caused maximal inhibition of carbon tetrachloride (CCl_4)-induced fibrosis, whereas EGFR-KO alone had modest effect.[13] Further, only double deletion of EGFR and MET aggravated CCl_4-induced liver injury, whereas EGFR-KO alone had no effect.[14] Future studies will be directed to investigate effects on the MASLD phenotype in EGFR/ErbB3 DKO and EGFR/MET DKO mice.

Although the pan-ErbB inhibitor, Canertinib, caused elimination of most of the hepatic lipid accumulation in EGFR-KO mice, this did not occur in the immediate pericentral hepatocytes surrounding the central lobular veins. However, overall removal of steatosis by Canertinib in EGFR-KO vs WT mice was comparable as reflected in total liver triglycerides analysis. Nevertheless, EGFR might still be independently regulating some of the phenotypic effects of Canertinib, which are not compensated by the other ErbB receptors. This was evident by the fact that 44% of the genes (1734 out of 3964) significantly altered by Canertinib in FFD-fed WT mice remain unaffected by Canertinib treatment in FFD-fed EGFR-KO mice, indicating that these genes were regulated by Canertinib in an EGFR-dependent manner. In contrast, 562 genes were differentially expressed by Canertinib only in EGFR-KO mice but not in WT mice. These genes were enriched in lipid metabolism/collagen biosynthesis processes, indicating that Canertinib might be utilizing a different set of genes in EGFR-KO conditions to produce effects on the MASLD phenotype similar to WT mice.

One of the most consistent and surprising findings in our study was increased fibrosis in the hepatocyte-specific EGFR-KO mice. Effects on hepatic fibrosis/stellate cell activation and TGF-β signaling pathways were observed not only in the 2- and 5-month FFD studies, but also in the chow-diet studies (ie, at the basal level), with actual increase in fibrosis after 5 months in EGFR-KO mice. This was surprising as previous studies (including our study) utilizing different EGFR inhibitors and diverse chronic liver injury models (including HFD, FFD, and CCl_4) showed decreased fibrosis by EGFR inhibition.[9,11,15] The differences might be due to the fact that EGFR signaling in stellate cells has been reported to promote fibrosis,[16,17] which might govern the overall response after systemic EGFR inhibition, whereas hepatocyte-specific EGFR may be protective against fibrosis. Our data, for the first time, demonstrates that EGFR signaling in hepatocytes is important to maintain an inhibitory effect on neighboring stellate cells, and absence of this signal results in stellate cell activation and fibrosis. It will be interesting to investigate how EGFR deletion in hepatocytes is communicated to stellate cells. Several of the TGF-β and PDGF ligands were induced in hepatocyte-specific EGFR-KO mice in our study, which might have a role to play in this cell-cell communication and will be further investigated in future. Along with changes in fibrosis signaling, our transcriptomic analysis also indicated alteration in several mediators involved in inflammatory response in EGFR-KO mice in both the 2- and 5-month studies, which might be relevant in the context of progression of steatosis to MASH and needs further investigation.

The overall observed differences and similarities between EGFR-KO and WT mice in the signaling activated during hepatic steatosis demonstrate the complexity of hepatocyte pathways mustered by the cell in the presence of regulatory obstacles to achieve similar results. The maintenance of the steatotic phenotype in the absence of EGFR by alternative signaling pathways is a perfect example of the "cybernetic" flexibility of hepatocyte networks employed to overcome obstacles and maintain complex phenotypes. Similar situations have been described in the context of liver regeneration, in which elimination of some of the key involved receptors and regulators never eliminate regeneration, which is always achieved, even with delays.[7,18] Such pathways may or not be similar, however, in the different inbred mouse strains.[19] An open approach to such differences should be relevant, though not always possible to employ, given the underlying difficulties of repeating experiments in multiple mouse strains. Sex differences related to EGFR need also to be eventually considered, given the fact that male mice express much higher number of EGFR receptors in hepatocytes compared with female mice.[20,21] The differences in zonal expression of ErbB receptors can also potentially influence outcomes in diverse fibrogenic models affecting different zones of liver as EGFR is more expressed in periportal lobular zone 1 and the proximal to zone 1 (a portion of zone 2), whereas Erbb3 has been shown to be expressed more in lobular zone 3.[14,22] Overall, EGFR expression is known to vary substantially in hepatocytes with various physiological factors such as age, feeding/fasting state, circadian cycles, and sex, which can potentially influence the phenotypes observed in studies utilizing EGFR deletion strategies or EGFR inhibitors using different models.[20,23]

Figure 10. (***See previous page***). **Pan-ErbB receptor inhibitor, Canertinib, prevented steatosis in EGFR-KO mice**. (*A*) Representative photomicrographs of Oil Red O (*upper panel*) and H&E (*lower panel*) stained liver sections at 2 months in various groups (WT-FFD, KO-FFD, Canertinib-treated WT-FFD, and Canertinib-treated KO-FFD). (*B*) Bar graphs showing liver TGs in various groups. Heat map showing comparative analysis of relevant (*C*) canonical signaling pathways and (*D*) upstream regulators predicted to be altered in EGFR-KO vs WT mice, Canertinib-treated WT vs WT mice, and Canertinib-treated KO vs WT mice, all fed FFD diet for 2 months. These heat-maps highlight that growth factor signaling (ErbB and ErbB2-ErbB3 signaling) along with downstream MAPK signaling (ERK, RAF, PI3K, AKT) were predicted to be inhibited only in Canertinib groups, but not in EGFR-KO alone group. (*E*) Venn diagram showing overlap of differentially expressed genes in Can-FFD-WT/FFD-WT vs Can-FFD-KO/FFD-KO groups. (*F*) Canonical signaling pathways and (*G*) biological processes (GO term) predicted to be enriched in DEGs exclusively from Canertinib-treated KO-FFD vs KO-FFD analysis, which were not present in Canertinib-treated WT-FFD vs WT-FFD analysis. n = 3–4 mice/group.

Table 8. Top Genes That Were Exclusively Up-regulated and Down-regulated in Can-EGFR-KO-FFD vs EGFR-KO-FFD, but not in Can-WT-FFD vs WT-FFD Groups

Up gene	Can-EGFR-KO/ EGFR-KO (FFD)	*P* value	Can-WT/ WT (FFD)	*P* value	Down gene	Can-EGFR-KO/ EGFR-KO (FFD)	*P* value	Can-WT/ WT (FFD)	*P* value
B4galnt4	9.2	.019	0.8	.649	Chrna4	0.22	.028	1.18	.402
Tmc3	7.1	.010	0.7	.515	Msmo1	0.53	.014	1.37	.187
Fam196a	5.4	.022	1.1	.930	Gm10642	0.26	.018	0.87	.706
Tex14	4.9	.009	0.7	.517	Sycp3	0.38	.020	0.98	.949
Ltb4r1	3.3	.004	1.2	.127	1810008I18Rik	0.40	.000	0.92	.669
Acnat2	3.1	.001	1.2	.282	Myom1	0.41	.045	1.04	.912
Hsbp1l1	3.0	.002	0.9	.760	Gm26608	0.46	.002	1.10	.708
Ms4a6c	2.7	.007	1.2	.281	Hmgcr	0.47	.001	0.95	.851
Pmaip1	2.7	.009	1.2	.496	Gm11992	0.47	.049	0.89	.745
Nos1ap	2.6	.014	1.1	.115	Cbarp	0.48	.033	0.92	.764
Fpr1	2.5	.000	1.2	.400	Tspan6	0.48	.027	1.08	.911
Rasl10b	2.5	.035	0.8	.549	Ptgis	0.50	.001	0.88	.610
Hck	2.5	.006	1.2	.400	Snai2	0.51	.022	0.84	.480
Ces4a	2.3	.037	1.1	.946	Inhbb	0.54	.045	1.02	.930
Tmem26	2.2	.027	1.0	.889	Ip6k2	0.54	.030	0.99	.963
Rhoh	2.2	.041	1.0	.956	Mblac2	0.55	.002	0.82	.185
Siglece	2.2	.005	1.2	.566	AI480526	0.55	.008	0.86	.394
Bcl3	2.1	.000	1.1	.306	Cyp51	0.55	.016	1.17	.310
St6galnac4	2.1	.006	1.2	.165	Atg16l2	0.56	.000	1.17	.337
Serpina3i	2.1	.014	1.2	.853	Arhgef37	0.56	.047	0.84	.408
Scimp	2.0	.033	1.0	.903	Klhl8	0.56	.046	0.86	.471
B430306N03Rik	2.0	.016	1.1	.777	Ggt5	0.57	.017	0.87	.371
Cd274	2.0	.011	1.2	.488	Gm10076	0.58	.034	1.22	.591
Kcna2	1.9	.001	1.0	.970	Ackr1	0.58	.047	1.03	.890
Spi1	1.9	.011	1.1	.585	4732419C18Rik	0.58	.002	1.24	.395
Rac2	1.9	.033	0.9	.766	Phc1	0.59	.000	0.82	.297
Serpina3g	1.8	.034	1.1	.586	Angpt2	0.59	.047	0.94	.809
Arl6	1.8	.024	1.1	.600	Samd14	0.59	.010	0.88	.251
Adrb1	1.8	.020	0.8	.527	B3gnt8	0.60	.048	0.90	.577
Ripk3	1.7	.044	1.1	.777	Snx32	0.60	.009	0.97	.845
Tmem268	1.7	.002	1.2	.181	Pcsk9	0.61	.011	1.20	.144
Cmpk2	1.7	.046	1.2	.509	Khnyn	0.61	.008	0.92	.346
Gbp7	1.7	.034	1.1	.306	Tctex1d4	0.26	.002	1.38	.460
Ackr4	1.7	.038	0.9	.309	Mmab	0.62	.004	0.92	.429
Adam23	1.7	.020	1.0	.919	Zscan20	0.62	.041	0.95	.772
Tmem161b	1.7	.008	1.2	.188	Ttc27	0.63	.009	0.88	.360
Lmo2	1.6	.028	1.2	.136	Mapk1ip1	0.64	.006	0.97	.848
Atp8b4	1.6	.041	1.2	.279	Irf2bp2	0.64	.037	0.97	.845
Themis2	1.6	.013	1.0	.953	Polr3gl	0.65	.015	0.82	.305
Mitd1	1.6	.010	1.1	.272	A530017D24Rik	0.65	.004	0.93	.657
Ppan	1.6	.036	1.0	.951	AA986860	0.66	.010	1.22	.509
Atp8b5	1.5	.013	0.7	.333	Ccng2	0.66	.006	0.92	.608
Slc10a1	1.5	.027	1.2	.420	Gm40787	0.66	.015	1.07	.892
Diablo	1.5	.015	1.0	.937	Slc19a2	0.66	.008	1.00	.992
Scn1b	1.5	.024	1.2	.448	Mterf2	0.66	.008	1.13	.647

Can, Canertinib; EGFR-KO, hepatocyte-specific deletion of EGFR; FFD, fast-food diet; WT, wild-type.

Table 9. List of DEGs Under Selected Biological Process Enriched in Gene Set Exclusively Altered by Canertinib in FFD-fed EGFR-KO Mice but not in FFD-fed WT Mice

S. No.	Altered biological process in 2-month study	Gene symbol
1	Lipid metabolic processes	Dhcr24, Hmgcr, Bscl2, Nsdhl, St3gal4, Ugcg, Xbp1, Acsl3, Acsm2, Acss2, Acot7, Acnat2, Angptl4, Alox5, Ces1g, Cyp4a10, Cyp51, Enpp6, Fads1, Hsd17b6, Ip6k2, Insig1, Lpin1, Mblac2, Msmo1, Mvd, Nfe2l1, Prdx6, Plpp1, Pcsk9, Ptgis, Rdh11, Sdsl, Thrsp, Tmem43
2	Cholesterol metabolic processes	Dhcr24, Hmgcr, Cln8, Nsdhl, Ces1g, Cyp51, Insig1, Msmo1, Mvd, Nfe2l1, Pcsk9, Saa1

DEG, Differentially expressed genes; EGFR-KO, hepatocyte-specific deletion of EGFR; FFD, fast-food diet; WT, wild-type.

In conclusion, hepatocyte-specific EGFR deletion did not have any major impact on steatosis, but enhanced fibrosis in the FFD model of MASLD. Our study, for the first time, to our knowledge, utilizes hepatocyte-specific gene deletion approach in adult mice to investigate the role of EGFR in MASLD and revealed a protective role of EGFR in hepatocytes on liver fibrosis. Further, gene networks associated with lipid metabolism were greatly impacted in EGFR-KO mice, but phenotypic effects might be compensated by alternate growth factor signaling pathways.

Materials and Methods

Experimental Setup and Mouse Models

$EGFR^{flox/flox}$ mice were obtained from the Mutant Mouse Resource & Research Centers (MMRRC; RRID: MMRRC_031765-UNC). Eight-week-old male $EGFR^{flox/flox}$ mice were administered a single dose of adeno-associated virus (AAV)8.TBG.PI.Cre.rBG (2.5×10^{11} viral particles per mouse, intra-peritoneally [ip]) vector to achieve hepatoctye-specific EGFR-KO. AAV8-TBG-CRE vector expresses CRE

Table 10. The KEGG Pathways and the Reactome Pathways Predicted to be Altered in Exclusive DEGs From Canertinib-treated KO-FFD/KO-FFD vs Canertinib-treated WT-FFD/WT-FFD

KEGG pathway	Gene count	*P*-value
Metabolic pathways	67	3.90E−05
Adherens junction	9	2.30E−03
Steroid biosynthesis	4	1.30E−02
Transcriptional misregulation in cancer	12	2.80E−02
Glutathione metabolism	6	3.60E−02
Retinol metabolism	7	3.70E−02
p53 signaling pathway	6	3.80E−02
Apoptosis - multiple species	4	4.70E−02
Reactome pathway	**Gene count**	***P*-value**
Cholesterol biosynthesis	7	1.20E−04
Metabolism of steroids	11	3.80E−03
Metabolism	71	4.10E−03
PTK6 promotes HIF1A stabilization	3	1.20E−02
Metabolism of lipids	28	2.60E−02
Signaling by TGFB family members	8	2.70E−02
SCF(Skp2)-mediated degradation of p27/p21	6	3.30E−02
p53-Dependent G1 DNA damage response	6	4.20E−02
p53-Dependent G1/S DNA damage checkpoint	6	4.20E−02
RUNX1 regulates transcription of genes involved in differentiation of HSCs	6	4.60E−02
Cell death signaling via NRAGE, NRIF and NADE	6	4.60E−02
G1/S DNA damage checkpoints	6	4.60E−02
MAP3K8 (TPL2)-dependent MAPK1/3 activation	3	4.80E−02
Cellular response to chemical stress	10	4.80E−02

DEG, Differentially expressed genes; EGFR-KO, hepatocyte-specific deletion of EGFR; FFD, fast-food diet; KEGG, Kyoto Encyclopedia of Genes and Genomes; WT, wild-type.

under thyroxine binding globulin (TBG) promoter, which is a hepatocyte-specific promoter. AAV8.TBG.PI.eGFP.WPRE .bGH8 (2.5×10^{11} viral particles per mouse, ip) administered to littermate $EGFR^{flox/flox}$ mice served as WT controls. AAV.TBG.PI.Cre.rBG (Addgene viral prep # 107787-AAV8) and pAAV.TBG.PI.eGFP. WPRE.bGH (Addgene viral prep # 105535-AAV8) were gifted from James M. Wilson. Starting the day of AAV8 injections, both AAV8-TBG-CRE and AAV8-TBG-GFP-treated mice were fed ad-libitum with either a chow diet or an FFD (ENVIGO #TD. 88137), characterized by high saturated fats (21% by weight; 42% kcal from fat), high cholesterol (0.2%), and high carbohydrates (sucrose: 34% by weight), complemented by a high-fructose-glucose solution in drinking water (d-glucose: 18.9g/L and d-fructose: 23.1g/L).[9,24] All animals (n = 3–5/ group) were harvested at 2 and 5 months after the start of FFD/chow feeding. For pan-ErbB inhibition studies, Canertinib was administered in FFD for 2 months at an estimated dose of 80 mg/kg/day, as used earlier.[7,9]

Housing and Ethical Considerations

The study adhered to strict housing conditions under a 12-hour light/dark cycle at the University of Pittsburgh's AAALAC-accredited facilities. All procedures were approved by the Institutional Animal Care and Use Committee, ensuring ethical treatment and humane euthanasia methods.

Glucose and Insulin Tolerance Tests

Glucose and insulin tolerance tests were conducted to assess metabolic dysfunction. The glucose tolerance test involved an 8-hour fasting followed by dextrose injection (2 g/kg, ip; in sterile phosphate buffered saline [PBS]), with glucose levels measured at 0, 15, 30, 60, 90, and 120 minutes. For the insulin tolerance test, mice were fasted for 4 hours, then injected with human regular insulin (0.75 U/ kg, ip; in sterile PBS), with subsequent glucose level monitoring at 0, 15, 30, 60, and 90 minutes.

Blood Parameters and Histological Analysis

Blood samples were processed to collect serum, which were analyzed for ALT, AST, cholesterol, and triglycerides. Paraffin-embedded liver sections were used for H&E and Sirius Red staining. Sirius Red stain was prepared by mixing 0.5 g Direct Red 80 (#365548; Sigma-Aldrich) in 1 L saturated solution of picric acid. Sections were deparaffinized and hydrated and stained in Sirius Red. Slides were then washed in acidified water, dehydrated in ethanol, and cleared before mounting. Frozen sections were used for Oil Red O staining, using Oil Red O Stain Kit (# KTORO EA; StatLab) as per manufacturer instruction. Immunohistochemistry for Ki67 (Cell Signaling #12202, dilution 1:500) and α-SMA (Cell Signaling #19245, dilution 1:300) were performed to assess cell proliferation and activation of stellate cells, respectively. The TUNEL assay (Apop-Tag Peroxidase In Situ Apoptosis Detection Kit S7100; Chemicon International Inc) was used to detect DNA damage. The assays were conducted by adhering to the guidelines provided by the manufacturer. Quantification of Sirius Red, α-SMA, TUNEL, and Ki67 stained sections was performed using at least 3 images per mouse liver by determining percentage positive stained area or percentage positive cell count utilizing Image J.

Liver TG Assay

Liver TG levels were quantified following the method outlined by Mooli et al.[25] In brief, frozen liver tissues from mice (~40 mg) were homogenized in 3 mL of a chloroform: methanol (2:1) solution in glass vials and thoroughly vortexed. The homogenate was incubated at room temperature for 90 to 120 minutes on a rotating shaker with intermittent vortexing. Later, the homogenate was acidified with 1 mol/L H_2SO_4, and centrifuged at 1000 rpm for 10 minutes at room temperature. The lipid fractions in the lower organic phase were collected and transferred to clean glass vials. A small aliquot (50 μL) of the lipid fraction was transferred to a new glass vial and completely evaporated. TG levels were then measured using the colorimetric Infinity Triglyceride Reagent (Thermo Fisher Scientific) and normalized to liver weight.

Protein Extraction and Western Blot Analysis

Total cell lysates made in RIPA buffer were separated by sodium dodecyl sulfate polyacrylamide gel electrophoresis in 4% to 12% NuPage Bis-Tris gels with 1× MOPS buffer (Invitrogen), then transferred to Immobilon-P membranes (Millipore) in NuPAGE transfer buffer containing 10% methanol. The nuclear lysates were obtained from freshly collected liver samples using the subcellular protein fractionation kit for tissues (# 87790 by Thermo Fisher Scientific), adhering to the provided instructions. All primary and secondary antibodies were obtained from Cell Signaling Technologies, unless stated otherwise. 1:1000 dilution was used for all primary antibodies and 1:2000 for all secondary antibodies, unless stated otherwise. SREBP-1 (1:200 dilution; Cat. # sc-13551) and PPARα (1:200 dilution; Cat. # sc-9000) antibodies were purchased from Santa Cruz Biotechnology, and HNF4α (1:1000; Cat. # PP-H1415-00) antibody was purchased from R&D Systems.

Cell signaling antibodies were EGFR (# 2646S), p-EGFR (# 2234S), GAPDH (# 5174S), FASN (# 3180s), ACC (# 3676S), ACLY (# 4332S), PPARγ (# 2435S), ErbB-3 (# 12708S), ErbB-2 (# 2165S), p-AKT (# 9271S), AKT (# 9272S), ERK-1/2 (# 4695), p-ERK-1/2 (# 4370), p-38 (# 9212), p-p38 (# 4092), JNK-1/2 (# 3708S), p-JNK-1/2 #4668S), SCD-1 (# 2794S), MET (# 4560S), p-MET (# 3133S), and β-actin-HRP (# 12262S).

RNA Isolation, Sequencing and Data Analysis

Total RNA was extracted from individual liver samples utilizing the Trizol method following the guidelines provided by Sigma and was then submitted to Novogene for quality verification, library preparation, sequencing and alignment to mouse reference genome mm10 (using STAR program). The RNA sequencing data have been deposited at SRA database with BioProject accession number PRJNA1093138. DEGs with significant expression changes were further analyzed using IPA (version 76765844;

Ingenuity Systems) or DAVID (version 6.8; Frederick National Laboratory). In addition to statistical criteria, change in expression by at least 1.3-fold (either upregulated or downregulated) was used for filtering DEGs. IPA was used for predicting altered canonical signaling pathways and upstream regulators based on changes in expression of downstream signature genes. Comparative analysis was performed using IPA to compare multiple experimental conditions. DAVID software was used for identifying enriched biological processes (GO terms), as well as KEGG and Reactome pathways, by comparing DEGs against the Mus musculus reference gene list.

Statistical Methods

Data are presented as mean ± standard error of the mean (SEM). The Student *t*-test and analysis of variance (ANOVA) with Tukey's post-hoc test were used for statistical comparisons, with significance considered at $P < .05$. The difference among groups were considered statistically significant at $^{*}P < .05$, $^{**}P < .01$, $^{***}P < .005$, and $^{****}P < .001$.

References

1. Asrani SK, Devarbhavi H, Eaton J, Kamath PS. Burden of liver diseases in the world. J Hepatol 2019;70:151–171.
2. Chan WK, Chuah KH, Rajaram RB, Lim LL, Ratnasingam J, Vethakkan SR. Metabolic dysfunction-associated steatotic liver disease (MASLD): a state-of-the-art review. J Obes Metab Syndr 2023;32:197–213.
3. Barb D, Portillo-Sanchez P, Cusi K. Pharmacological management of nonalcoholic fatty liver disease. Metabolism 2016;65:1183–1195.
4. Bhushan B, Michalopoulos GK. Role of epidermal growth factor receptor in liver injury and lipid metabolism: emerging new roles for an old receptor. Chem Biol Interact 2020;324:109090.
5. Doring P, Pilo GM, Calvisi DF, Dombrowski F. [Nuclear Her2 expression in hepatocytes in liver disease]. Pathologe 2017;38:211–217.
6. Scheving LA, Zhang X, Garcia OA, et al. Epidermal growth factor receptor plays a role in the regulation of liver and plasma lipid levels in adult male mice. Am J Physiol Gastrointest Liver Physiol 2014;306:G370–G381.
7. Paranjpe S, Bowen WC, Mars WM, et al. Combined systemic elimination of MET and epidermal growth factor receptor signaling completely abolishes liver regeneration and leads to liver decompensation. Hepatology 2016;64:1711–1724.
8. Lopez-Luque J, Caballero-Diaz D, Martinez-Palacian A, et al. Dissecting the role of epidermal growth factor receptor catalytic activity during liver regeneration and hepatocarcinogenesis. Hepatology 2016;63:604–619.
9. Bhushan B, Banerjee S, Paranjpe S, et al. Pharmacologic inhibition of epidermal growth factor receptor suppresses nonalcoholic fatty liver disease in a murine fast-food diet model. Hepatology 2019;70:1546–1563.
10. Choung S, Kim JM, Joung KH, Lee ES, Kim HJ, Ku BJ. Epidermal growth factor receptor inhibition attenuates non-alcoholic fatty liver disease in diet-induced obese mice. PLoS One 2019;14:e0210828.
11. Liang D, Chen H, Zhao L, et al. Inhibition of EGFR attenuates fibrosis and stellate cell activation in diet-induced model of nonalcoholic fatty liver disease. Biochim Biophys Acta Mol Basis Dis 2018;1864:133–142.
12. Xu Y, Zhu Y, Hu S, et al. Hepatocyte nuclear factor 4alpha prevents the steatosis-to-NASH progression by regulating p53 and bile acid signaling (in mice). Hepatology 2021;73:2251–2265.
13. Scheving LA, Zhang X, Threadgill DW, Russell WE. Hepatocyte ERBB3 and EGFR are required for maximal CCl4-induced liver fibrosis. Am J Physiol Gastrointest Liver Physiol 2016;311:G807–G816.
14. Scheving LA, Zhang X, Stevenson MC, Threadgill DW, Russell WE. Loss of hepatocyte EGFR has no effect alone but exacerbates carbon tetrachloride-induced liver injury and impairs regeneration in hepatocyte Met-deficient mice. Am J Physiol Gastrointest Liver Physiol 2015;308:G364–G377.
15. Fuchs BC, Hoshida Y, Fujii T, et al. Epidermal growth factor receptor inhibition attenuates liver fibrosis and development of hepatocellular carcinoma. Hepatology 2014;59:1577–1590.
16. Perugorria MJ, Latasa MU, Nicou A, et al. The epidermal growth factor receptor ligand amphiregulin participates in the development of mouse liver fibrosis. Hepatology 2008;48:1251–1261.
17. Komposch K, Sibilia M. EGFR signaling in liver diseases. Int J Mol Sci 2015;17:30.
18. Michalopoulos GK, Bhushan B. Liver regeneration: biological and pathological mechanisms and implications. Nat Rev Gastroenterol Hepatol 2021;18:40–55.
19. Rinella ES, Threadgill DW. Efficacy of EGFR inhibition is modulated by model, sex, genetic background and diet: implications for preclinical cancer prevention and therapy trials. PLoS One 2012;7:e39552.
20. Benveniste R, Danoff TM, Ilekis J, Craig HR. Epidermal growth factor receptor numbers in male and female mouse primary hepatocyte cultures. Cell Biochem Funct 1988;6:231–235.
21. Wang L, Xiao J, Gu W, Chen H. Sex difference of EGFR expression and molecular pathway in the liver: impact on drug design and cancer treatments? J Cancer 2016;7:671–680.
22. Carver RS, Stevenson MC, Scheving LA, Russell WE. Diverse expression of ErbB receptor proteins during rat liver development and regeneration. Gastroenterology 2002;123:2017–2027.
23. Scheving LA, Tsai TH, Cornett LE, Feuers RJ, Scheving LE. Circadian variation of epidermal growth factor receptor in mouse liver. Anat Rec 1989;224:459–465.
24. Charlton M, Krishnan A, Viker K, et al. Fast food diet mouse: novel small animal model of NASH with ballooning, progressive fibrosis, and high physiological fidelity to the human condition. Am J Physiol Gastrointest Liver Physiol 2011;301:G825–G834.

25. Mooli RGR, Rodriguez J, Takahashi S, et al. Hypoxia via ERK signaling inhibits hepatic PPARalpha to promote fatty liver. Cell Mol Gastroenterol Hepatol 2021;12:585–597.

Received March 28, 2024. Accepted July 16, 2024.

Correspondence
Address correspondence to: Bharat Bhushan, MS, PhD, DABT, Department of Pathology, School of Medicine, University of Pittsburgh, 200 Lothrop St, South BST S408, Pittsburgh, PA 15261. e-mail: bhb14@pitt.edu.

CRediT Authorship Contributions

Shehnaz Bano (Formal analysis: Equal; Investigation: Equal; Methodology: Equal; Writing – original draft: Equal; Writing – review & editing: Equal)

Matthew Copeland (Formal analysis: Equal; Investigation: Equal; Methodology: Equal)

John Stoops (Investigation: Supporting)

Anne Orr (Investigation: Supporting)

Siddhi Jain (Formal analysis: Supporting)

Shirish Paranjpe (Methodology: Supporting)

Raja Gopal Reddy Mooli (Investigation: Supporting)

Sadeesh K. Ramakrishnan (Investigation: Supporting)

Joseph Locker (Data curation: Equal; Formal analysis: Equal)

Wendy Mars (Methodology: Supporting)

George Michalopoulos (Funding acquisition: Equal; Writing – review & editing: Supporting)

Bharat Bhushan (Conceptualization: Lead; Data curation: Lead; Formal analysis: Equal; Funding acquisition: Lead; Investigation: Equal; Methodology: Equal; Project administration: Lead; Supervision: Lead; Writing – original draft: Equal; Writing – review & editing: Lead)

Conflicts of interest
The authors disclose no conflicts.

Funding
This study was supported by National Institutes of Health (NIH) R01 DK122990, NIH R01 DK135566, and by the Cleveland Foundation; Additional support provided by NIH grant P30 DK120531 to Pittsburgh Liver Research Center (PLRC).